Final Technical Report
U.S. Geological Survey
National Earthquake Hazards Reduction Program
USGS External Award # G18AP00065 and #G18AP00066

Collaborative Research with University of South Florida and University of Cincinnati: Determining Slip Rates for Camp Rock Fault (Eastern California Shear Zone) using Terrestrial Cosmogenic Nuclide Dating

Paula Marques Figueiredo & Lewis A. Owen
(Previously at Department of Geology, University of Cincinnati, OH)
Marine, Earth and Atmospheric Sciences
North Carolina State University
2800 Faucette Drive, 1125 Jordan Hall
Raleigh, NC 27695

paula_figueiredo@ncsu.edu, lewis.owen@ncsu.edu

Paul H. Wetmore and Timothy H. Dixon
NES 107
School of Geosciences
University of South Florida
Tampa, FL 33620
wetmore@usf.edu, thd@usf.edu

Craig Rasmussen
Department of Environmental Science
University of Arizona
Tucson, AZ 85719
crasmuss@cals.arizona.edu

Research supported by the U.S. Geological Survey (USGS), Department of Interior, under USGS award number G18AP00065 & G18AP00066. The views and conclusions contained in this document are those of the authors and should not be interpreted as representing the opinions or policies of the U.S. Geological Survey. Mention of trade names or commercial products does not constitute their endorsement by the U.S. Geological Survey.

Abstract

The Camp Rock-Emerson-Copper fault system is one of the main NW trending, dextral strike-slip faults in the Eastern California Shear Zone (ECSZ) in the Mojave Desert. The majority of the geologic slip-rates in ECSZ have been estimated from the displacements of geologic and geomorphic features, generally younger than 100 ka, and yield a range from 0.04±0.2 to 1.8±0.3 mm/a, with the exception of the Calico fault than has a slip rate of 3.2±0.4 mm/a. To assess the importance of the Camp Rock-Emerson-Copper fault system within the ECSZ and its long-term slip rate, alluvial fan surfaces along the western flank of Rodman Mountains that are faulted by the Camp Rock and Emerson faults are dated using ^{10}Be and ^{36}Cl terrestrial cosmogenic nuclides. Dating results, together with geomorphic and soil characterization suggest two main generations of Pleistocene alluvial fan development at ~280 and >350 ka along the central and southern sections of the Camp Rock fault, respectively. The southern Camp Rock fault steps right laterally toward the Emerson fault bounding a graben and has a slip rate of ~0.6 mm/a based on a 638 ± 40 m offset of the older alluvial fan surface. Reconstructions of offsets for the younger alluvial fan surface along the Camp Rock fault north of the step with Emerson fault, indicate either ~300 or ~1350 m of displacement depending on how landforms are matched across the fault and indicating slip-rates of ~1.1 or ~4.9 mm/a, respectively. These calculations suggest a southward decrease in the Camp Rock fault slip rate, probably due to deformation partitioning with the Emerson fault. Despite ambiguous evidence for long-term displacement along the Camp Rock fault, the new results support the view that there are significant spatial and transient changes in slip rate along the Camp Rock-Emerson-Copper fault system. In addition, a significant portion of deformation within the Mojave section of ECSZ is taken up on this fault system. The numerical ages for Pleistocene surfaces are the first for this region.

1. Introduction

A major component for fault characterization for the purposes of seismic hazard assessment is the quantification of slip rates and their variability through time. Characterizing how the fault systems interact through space and time is crucial to the understanding of how the tectonic stress is accommodated and understanding how faults evolve at a regional scale. This characterization in tectonically active regions has further relevance since the mechanisms of fault interaction can promote the generation and/or a reactivation of preexistent structures producing earthquakes at locations and with magnitudes beyond the documented fault trace. The occurrence of earthquakes as the result of the interaction between fault systems is particularly important for the Eastern California Shear Zone (ECSZ) of the San Andreas-Gulf of California plate margin, where segments of some of the main NW-SE dextral strike-slip faults ruptured together during the 1992 M_w7.3 Landers and 1999 M_w7.1 Hector Mine earthquakes along with other unmapped faults (Sieh et al., 1993; Treiman et al., 2002 among others), and more recently for the for the 1999 Ridgecrest M_w 6.4 and 7.1 sequence (Ponti et al., 2020).

The compilation of paleoseismology data for the western Mojave section of ECSZ (MECSZ) do not show a similar rupture across the same fault segments that ruptured during the Landers earthquake, for the last 15–20 ka. The paleoseismic evidence suggesting that the Landers earthquake was not a characteristic rupture event. Nevertheless, in the southern part of the Landers surface rupture, paleoseismology trenching across several faults revealed previous surface ruptures that probably occurred simultaneously (Rockwell et al., 2000). This study suggests that earthquakes cluster every 4–5 ka on the faults of western MECSZ, and that they interact throughout the Holocene. Plate boundary scale interactions have also been suggested between the MECSZ and seismogenic structures in the greater Los Angeles basin area on either side of the San Andreas fault, where Holocene earthquake activity on one side of the San Andreas is synchronous with seismic quiescence in the other (Dolan et al., 2007). This natural complexity added to the intrinsic processes of fault evolution, growth, and propagation and increases the difficulty in recognizing the variability of regional stress and strain accommodation through time, and how those changes condition the slip rates for individual structures. To examine these complexities and other issues, we examine the Camp Rock-Emerson-Copper fault system, one of the main NW-trending dextral strike-slip faults in the MECSZ (Fig.1).

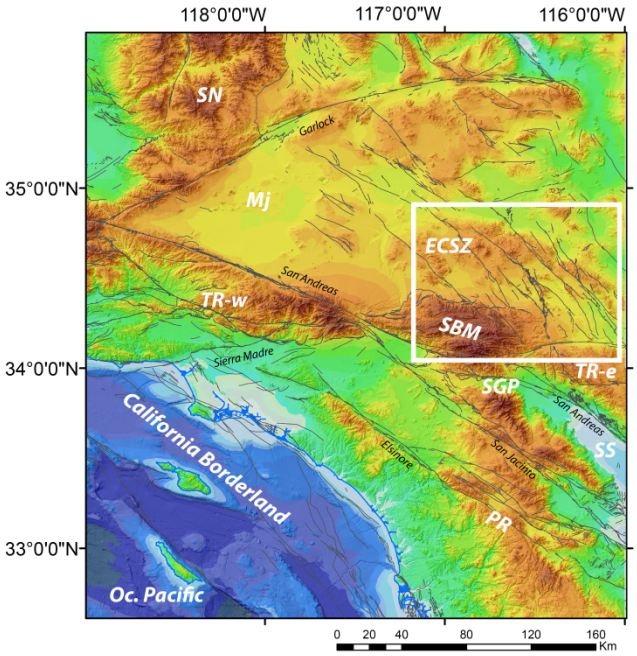

Figure 1. Digital elevation model (DEM) for southern California and off-shore between ~36°N to ~33°N. Main physiographic features and tectonic structures accommodating the North America-Pacific plate boundary on-going deformation are identified. The area within the white line is presented in detailed in Fig.2. SN- Sierra Nevada; Mj-Mojave; ECSZ- Eastern California Shear Zone; TR-w- western Transverse Range; SBM- San Bernardino Mountain; SGP- San Gorgonio Pass; TR-e – eastern Transverse Range; SS- Salton Sea; PR- Peninsular Range. DEM made from ASTER 30 m and US Coastal Relief Model - Southern California Version 2 30m and fault traces from the USGS Quaternary fault database.

Additional complexity in the stress accommodation mechanisms and fault behavior is also revealed through geodesy on 10–100 yr timescales. Data from geodesy is not consistent with the geological data for the MECSZ (e.g., McGill et al., 2015). This discrepancy between the known geologic slip rates and the measured geodetic slip rates for the MECSZ has long been recognized, even prior to the Landers and Hector Mine earthquakes, suggesting that the MECSZ may be experiencing a strain transient with faster geodetic than geologic rates (e.g., Sauber et al., 1994). The geodetic slip rates for the Mojave range from 10 to 14 mm/a or as high as 18 mm/a depending on the geodetic models (Savage et al., 1990; Sauber et al., 1994; Dixon et al., 1995, Spinler et al., 2010; McGill et al., 2015; Evans et al., 2016). However, cumulative geologic slip rates since the Late Pleistocene for the main active MECSZ at latitudes~34.5° to 35°N is ≤6.2±1.9 mm/a (Oskin et al., 2008). This slip rate is roughly half that of the geodetic rates, but geologic slip-rate should be regarded a minimum estimate because it does not include slip rates for active minor structures that have not been considered/studied across that transect.

Geodetic versus geology slip rates differences for an individual structure can be over/underestimated by the different modeling parameters and inversion methods (e.g., Herbert et al., 2014a). Effects resulting from post-seismic relaxation can also favor higher geodetic rates, leading to higher geodetic vs. geologic discrepancies by as much as ~2 mm/a. McGill et al. (2015) infer that the largest discrepancies between geological and geodetic rates in MECSZ are localized in the vicinity of the Landers and Hector Mine ruptures, namely along the Calico fault and can be due to additional nearby faults included in the geodetic modeling. The Calico fault, that did not rupture during the Landers or Hector Mine earthquakes has the greatest individual geological slip rate (1.8±0.7 mm/a) for the Late Pleistocene (Oskin et al., 2008) and for the last 350 ka (3.2±0.4 mm/a; Xie et al., 2018). This is corroborated by the geodetic work of Evans et al. (2016) who estimates a discrepancy of 5.8 mm/a for Calico fault that could not be simply justified by the 23% off-fault deformation (OFD) estimated by Shelef and Oskin (2010).

Models of how geological slip rates for some structures within MECSZ may have changed temporally and spatially add further questions to the discrepancies between geology and geodetic data. Dixon and Xie (2018) present a kinematic model for MECSZ since its inception (or acceleration) assuming a steady state condition with accommodation of 10–12 mm/a. In this model, the larger scale can be demonstrable as the Pacific-North America motion has been constant throughout the lifespan of the MECSZ. They propose an eastward motion of the MECSZ block that induces a transit through a stable and localized deep ductile dextral shear zone favoring the development of faults in the overlying brittle upper crust. This translation could explain why the highest total cumulative displacement is located to the eastern end of the fault (Bristol-Granite Mountains). The lack of Quaternary activity supports this hypothesis. The fault with highest slip rate is located in the center of the shear zone and has significantly less total displacement. This model proposes spatial and temporal variability that is systematically moving migrating through the network regardless of the long-term constant strain rate for the MECSZ. As such, the eastern active faults should have a lower slip-rate than the long-term geological slip-rate (as supported by the geodesy). However, such variability in space and time is yet to be corroborated by geologic data.

To our knowledge, a regional database of the geological slip rates including several fault systems other than the major ones, with slip rates obtained at different locations within fault systems, has not been acquired for the MECSZ. Such a database would enable the characterization of slip rates and changes in the structural complexity during different time ranges during the Quaternary. The majority of the regional geologic slip rates use one or more of the following:

1) Cenozoic geologic marker displacements (Dokka, 1983; Dokka and Travis, 1990; Andrew and Walker, 2017), which is conditioned by the timing for the inception of the displacements for which there is no consensus and in addition might had been diachronous (Woodburne, 2015 and references within; Miller, 2017 and references within; Andrew and Walker, 2017). These are a total cumulative displacement rather than a long-term slip rate.

2) Late Pleistocene (commonly <100 ka) to Holocene slip rates based on the displacement of late Quaternary geomorphic markers dated with geochronology methods (Oskin et al, 2008; Selander, 2015; Xie et al., 2018; Haddon et al., 2019).

3) Holocene to late Pleistocene paleoseismology data, conducted mainly along the Landers and Hector Mine ruptures zones providing deformation per paleoseismic event that can be used to estimate slip rate to be compared with slip rate inferred from geomorphology (Rockwell et al., 2000 and references within; Ganev et al., 2010).

Filling the gaps of the existing knowledge in the short- and long-term geological slip rates, as well as, improving the quantification of fault deformation through time, is necessary to comprehend the mechanisms and processes that condition surface slip deficit during a shear zone evolution. Refining the knowledge about the characteristics of surface deformation and geologic slip rates is, therefore, a critical issue. Quantified slip rates are most relevant at faults where the geodetic rates seem to be higher, namely at the center of shear zone such as Calico and Camp Rock faults. Our study therefore is aimed to define and understand the long-term slip rate of Camp Rock fault.

2.Camp Rock Fault

The Camp Rock-Emerson-Copper fault system (CREC) is one of the major fault systems in the MECSZ (Fig. 2). Similar to the other major faults in the MECSZ, it is predominantly dextral and trends NW. The CREC stretches for ~90 km and is located 11 to 14 km west of the Calico-Hidalgo fault system. The fault system has 3 distinct sections:1) a northern one located south of Barstow named the Camp Rock fault, which is ~25 km long with a well-defined linear trace; 2) the central section defined by the Emerson fault that steps through a right-releasing step-over zone that is ~2 km wide to the Camp Rock fault; and 3) the Copper Mountain fault, is ~20 km long and terminates just north of the Pinto Mountain Fault between the towns of Joshua Tree and Twentynine Palms.

The Emerson fault is the longest section of the CREC and can be subdivided into a northern sub-section, south of the Camp Rock fault that extends for ~25 km and is characterized by an anastomosing trace pattern (approximately along the Fry Mountains area), and a straighter southern sub-section that stretches for ~25 km long from the Emerson Lake area to Sand Hill. Beyond Sand Hill, the Emerson fault transfers to the straight discontinuous Copper Mountain fault, through a releasing step-over that is ~1 km wide and trends more to the south closer to the Pinto Mountain fault (Fig. 2).

The northern segment of the Camp Rock fault is located along the base of the western hillsides of the Newberry and Rodman mountains, displacing bedrock composed mainly of Mesozoic plutonic and hypoabyssal igneous rock that intrude Paleozoic metasedimentary rock that rarely outcrop near the Camp Rock fault. Sedimentary and volcanic rocks from the early Miocene Pickhandle Formation are present along the northern Newberry Mountains (Dibblee, 1964). Several faulted Quaternary alluvial fans and bajadas are present in the region providing markers to help define the magnitude of Quaternary deformation (Dibble, 1964: Bull, 1979). Most of the fault trace is straight and the fault zone is a few hundred meters wide. Occasionally there are two parallel strands; the fault is mainly vertical, with uplift to the east, although locally dipping to the west with a minor reverse component. The total displacement inferred for this structure is variable from 4.1 km based on a magnetic anomaly (Jachens et al., 2002) to 3.75 km based on an early Tertiary plutonic contact (Miller and Morton, 1980), to 1.6 km based on a volcanic-sedimentary rock contact with gneiss, diorite and granite (Hawkins, 1976), and to 1.2 km based on displaced alluvial fans (Dibble, 1964).

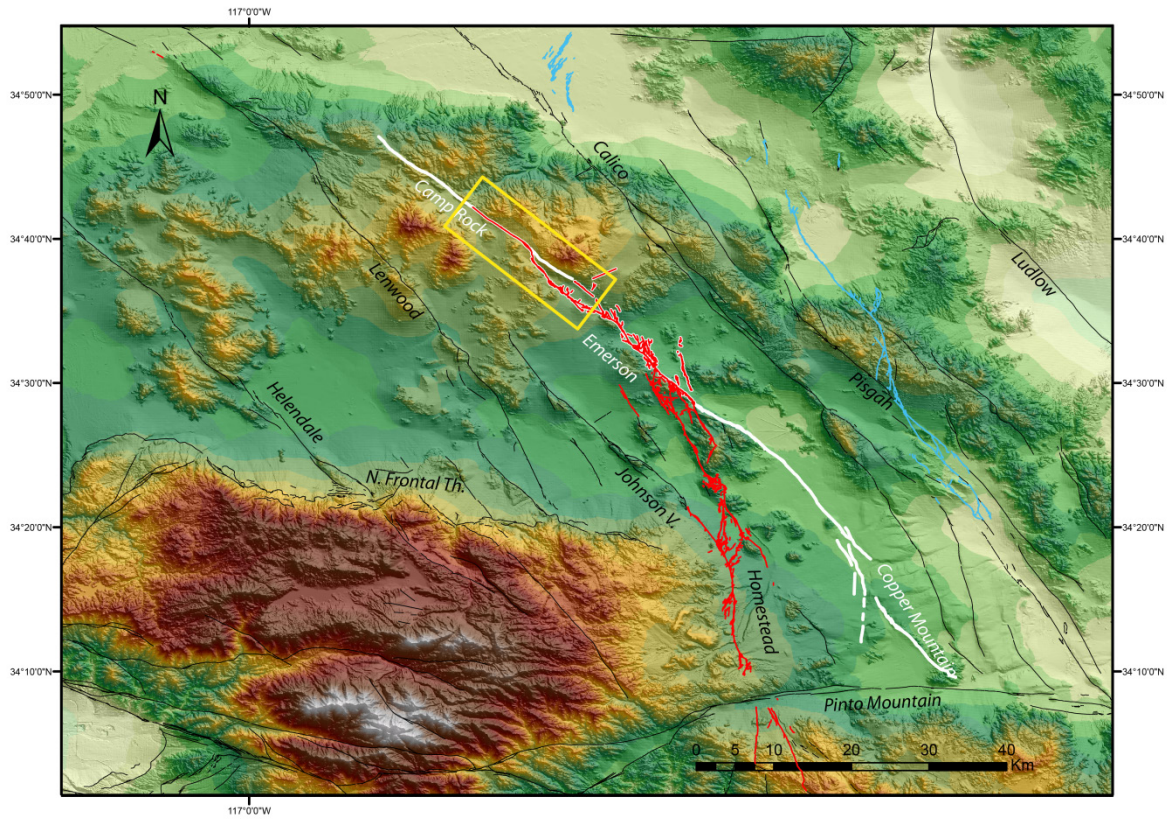

Figure 2. Main active faults in the Mojave section of the Eastern California Shear Zone. The Camp Rock-Emerson-Copper fault system is highlighted with a white trace; the 3 sections are labeled, Camp Rock, Emerson and Copper Mountain faults. The Landers and Hector Mine surface ruptures are highlighted by the red and blue traces, respectively. The study area is delimited by the box with yellow trace. Digital Elevation model made from ASTER 30 m and fault traces from the USGS Quaternary fault database.

A Quaternary displacement was initially estimated as part of geological mapping as being 0.8 km (Dibble, 1964) or 1.2 km (Hawkins, 1976), but there was no absolute dating of the offset markers. Later, geomorphic analyses and trenching across the fault trace served to define recent activity (Bull, 1979; Manson, 1986 and references within) with slip rate estimates between 1 and 3 mm/a, again estimated without absolute dating. Oskin et al. (2008) provides quantified slip-rate to be $\leq 1.4\pm0.6$ mm/a (for the last 50±20 ka) define by numerical dating. Herbert et al. (2014a) revises geodetic inversions models for fault slip along the Camp Rock fault by adjusting in the model of active fault traces undertaken by Jennings and Bryant (2010). Their results are approximately the same as the geologic slip rate defined by Oskin et al. (2008). However, Evans et al. (2016) proposes a geodetic rate of 0.5–4.7 mm/a, a much larger range indicating that Camp Rock fault also presents a significant discrepancy between geologic and geodesic rates.

The Camp Rock fault is a straight narrow fault zone, and as such is a structurally simple structure with probably low OFD. Analysis of the Landers surface rupture in the area of the Camp Mine by Milliner et al. (2015) suggests ≤20% OFD localized within a few meters from the main fault trace. This structural simplicity and low OFD, should favor similar geological and geodetic slip rates. In contrast, the fault complexity of the step-over between the Camp Rock and Emerson faults would promote significantly more OFD (as high as 80%) and hence the differences between geodetic and geological slip rates will be greater. Thus, the Camp Rock fault segment north of the step-over with Emerson fault should be an ideal place to compare geological and geodetic slip-rates.

2.1. Bedrock and Quaternary units

Several faulted Quaternary units were mapped by Dibble (1964, 1970) across the Camp Rock fault area (Fig.2). The Quaternary sequence from the bottom to top starts with the Older Valley Sediments of inferred Pleistocene age, that derived mainly from Tertiary units and are composed of fanglomerates and gravels (Qof) and clay and marl (Qoc). This basal unit generally lays unconformably on Tertiary and older units, is locally deformed and is strongly dissected. It is overlaid by an intermediate unit, the Older Alluvium (Qoa) of probable late to mid-Pleistocene age, which is derived from proximal highlands of different bedrock, and is characterized as bajadas and alluvial fans with different degrees of dissection. A younger sequence corresponds to recent deposits (latest Pleistocene to Holocene) such as alluvium (Qa), river sand (Qrs), fan gravel (Qf) and dune sands (Qs). The older and basal unit is only present near the northwestern end in the Daggett quadrangle (USGS I-592) and not southwards in the Rodman Mountains quadrangle (USGS I-430).

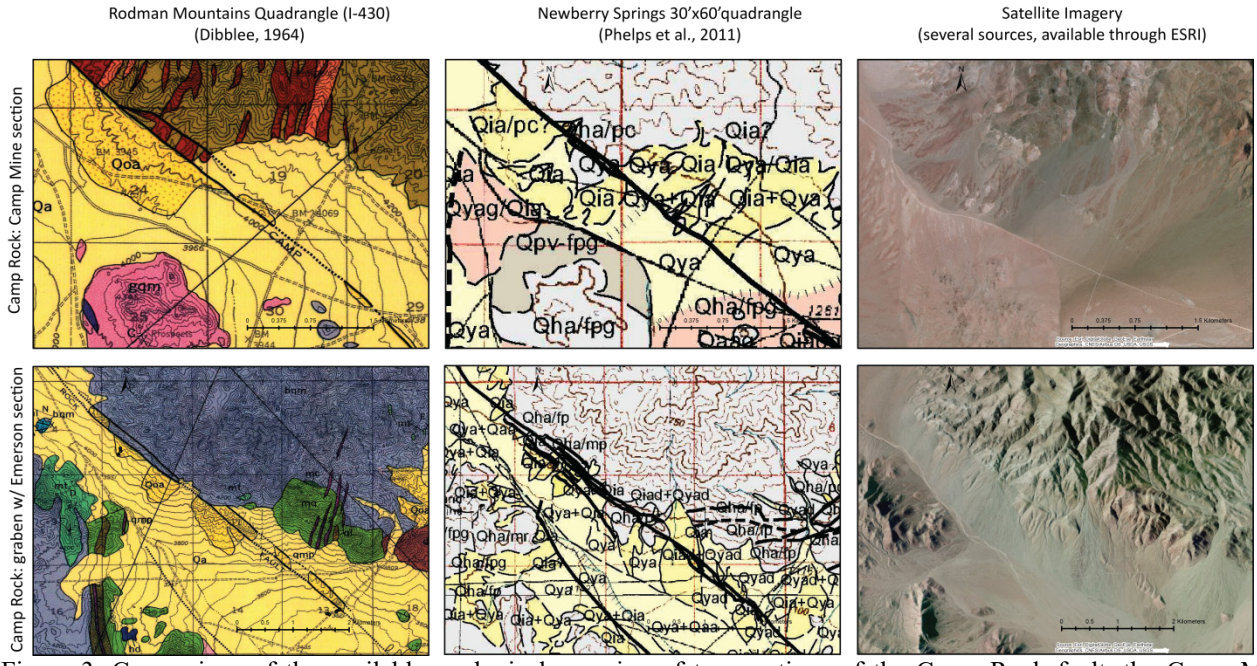

Figure 3. Comparison of the available geological mapping of two sections of the Camp Rock fault, the Camp Mine section and south of it the section parallel with Emerson, where a graben is formed due a releasing step-over. Satellite imagery is provided for reference. Scale is included in each image.

The bedrock in the Camp Mine area in the northern steep hill slopes is mainly latite porphyry (lp) with dikes of basalt porphyry (bp), and siliceous felsite and aplite (sf). Most of the lithologies in the northern Rodman Mountains are quartz-poor while at the southern hill slopes are shaped in older granitic rocks, namely biotite quartz monzonite (bpm) and granite and quartz monzonite (gpm). Hillslopes along the Camp Rock-Emerson fault are mainly composed of biotite quartz monzonite, although metaquartzite (mq), metaconglomerate (mc) and tactite (mc).

McFadden (1982) and Bull (1991, 1996) examined the Quaternary units of Dibble (1964) for the Mojave region and improve the chronology by analysis of soil development and relative surface development. Their work showed nine distinct surfaces although still organized as young, intermediate and old alluviums and without numerical ages. Later research, in most cases associated with the need to differentiate chronologies for active tectonic studies, used criteria such as desert pavement and desert varnish development, smoothing of swales and bars, degree of incision, soil geomorphology and surface dating using terrestrial cosmogenic nuclides (TCNs) to differentiate more piedmonts and alluvial fan surfaces, and tentatively correlating Pleistocene glacial and interglacial periods (SCAMP, 2000; Eppes et al., 2003;Oskin et al., 2007; Frankel et

al., 2008; Selander, 2015). These efforts resulted in more than twenty distinct Quaternary mappable units, which are not ubiquitous.
A review of the Quaternary mapping of Dibble (1964) along the Camp Rock fault is published in the Surficial Geologic Map of Newberry Springs 30' x 60' quadrangle (Phelps et al., 2011). The Older alluvial Qoa (late to mid-Pleistocene) in the northern extensional graben is revised as Qia keeping approximately the same geologic contacts. However, along the Camp Mine section and in the southern graben, the geologic mapping of units Qoa and Qa is revised as partially to be Qia, Qia+Qya and Qya (Fig.2). This leads to relevant differences with implications when measuring Quaternary displacement.

2.2. Evidence of active faulting

The surface rupture during the Landers earthquake provides the most recent and unequivocal evidence of tectonic activity related to the Camp Rock fault. The northern termination of this rupture occurred along an 8 km stretch of the Camp Mine fault (Fig. 2). The Camp Mine rupture is likely to have been statically triggered by the rupture along the adjacent Emerson fault (Kaneda and Rockwell, 2009). The reasoning for this assumption lies in the lack of aftershocks and for a shallow 3-km-deepfault plane failure. Holocene movement of the Camp Rock fault is inferred from channels and rills that are displaced right laterally by 1 to ≤ 10m.

Paleoseismology studies conducted in trenches provided minor evidence of earthquakes during the late Quaternary (Slemons, 1980). A small vertical displacement suggests an event occurred a few hundred to a few thousand years ago. An alluvial fan surface in the southern segment that is assumed to be early Holocene (8–12 ka), is not offset, suggesting that no Holocene faulting (Slemons, 1980). Unfortunately, the locations of the trenches are not described well enough to provide useful analysis. After the Landers earthquake, new paleoseismology efforts identified three earthquakes since 20 ka (Rockwell et al., 2000 and references within). An earthquake recurrence period is estimated to be 5–7 ka, with the penultimate earthquake at 9 ka, and maybe another at 2–3 ka.

A quantitative analysis of the geomorphic expression along the fault by Bull (1979) shows that the segment of the Camp Rock fault north of the Emerson fault is "highly active" (Class 1 of Bull 1979) with Holocene to Pleistocene activity. In contrast, the segment of the Camp Rock fault along the graben with the Emerson fault is "moderately active" (Class 2 of Bull 1979) with only Pleistocene faulting (Fig.3). Since there are no numerical ages for the faulted landforms, their activity and slip rates have not been defined.

2.3. Regional alluvial fan sequence

A succession of alluvial fan surfaces in the vicinity of the study area, along the Emerson fault, is described by Bull (1996). The youngest surfaces/units, Q4b and Qa4a, are argued to have formed after 4 ka. Two other pulses of Holocene aggradation are associated with surfaces/units Q3a (12–9.5 ka) and Q3b (9–6 ka), and pulses of late Pleistocene aggradation are associated with surface/unit Q2c (~55–70 ka, by correlation with data from Colorado and Southern California). Another pulse of aggradation is associated with surface/unit Q2b, which was inferred to have formed during marine isotope stage (MIS) 5 (~ 80–130 ka).Q2b is an important climate marker although it not confirmed by geochronology and only corroborated by relative soil dating (Bull, 1996). A regional Q2a surface/unit is argued to have formed 400–730 ka (in correlation with Colorado age control) and a regional Q1 surface/unit is argued to be >1200 ka (Bull, 1991). Although assuming a temporal and spatial regional variability, evidence for aggradation during Q2c (and maybe partially Q2b) may be provided by TCN alluvial fan ages in the Mojave ranging from 37±7 to 56±21 ka (Oskin et al., 2008), and possibility evidence for a Q2a dating is provided by a alluvial fan with a TCN age of 346±24 ka (Xie et al., 2018).

2.4. Geographic setting

The study area is located along the western foothill of the Rodman Mountains, along the eastern side of a~18-km-long and 2–3-km-wide NW trending valley. The elevation of the valley floor varies between 1200 and 1250 m above sea level (asl), and the mountain peaks reach elevations of~1800m asl.

The climate is arid, although moisture from Pacific Ocean moves east providing 10-30% humidity during the day and up to 50% humidity nighttime. Occasional storms occur mainly in summer creating flash floods. The annual average precipitation at Barstow is 13.5 cm/a. The annual average low temperature is 11°C while the annual average high temperature is 27°C, with temperatures occasionally reaching 35–40°C. Winds up to 120 km/h can occur, favoring dust storms with mobilization of fine particles and aeolian sediments (Western Region Climate Center, climate data for Barstow, http://www.wrcc.dri.edu). In the study area, the higher elevation can favor higher humidity, and the valley configuration wind protection from most directions, altogether potential relevant for the type of weathering and soil characterization.

3. Methods

We analyzed the geology and geomorphology, and the faulted alluvial fan surfaces in particular, to investigate geological slip rates along the Camp Rock fault. We divided Camp Rock fault study area in two sections, the "Camp Mine" study area that ruptured during Landers and the "Graben" study area which is the eastern bound in the right lateral releasing stepover with the Emerson fault (Fig. 4). Displacements were identified based on correlation of alluvial fan surfaces and ages were determined using TCN dating and soil characterization.

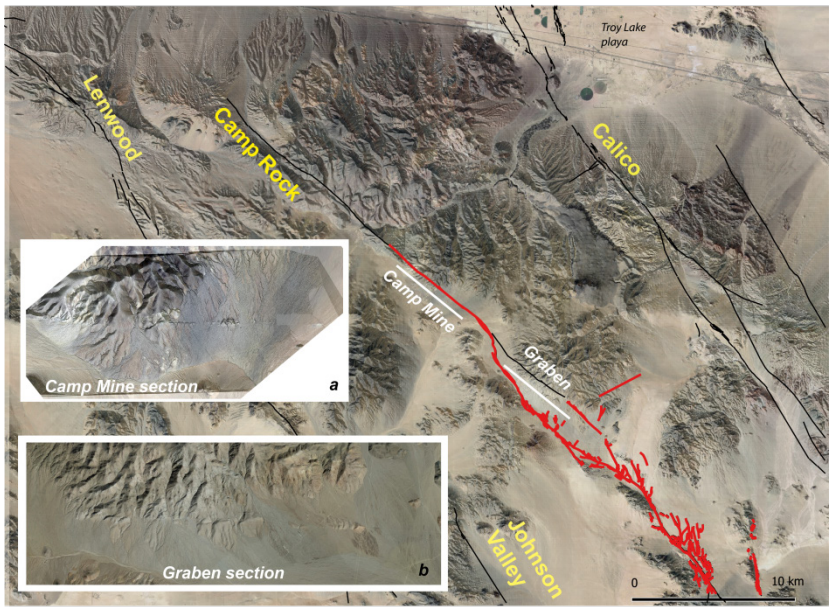

Figure 4. Location of Camp Rock fault detailed study areas, Camp Mine and Graben study areas. a) Camp Mine section, satellite imagery with Lidar DEM and b) Graben section Google Earth imagery. Satellite imagery over DEM (ALOS) and fault traces from the USGS Quaternary fault database. Landers earthquake surface rupture in red trace.

We conduct geomorphology analyses using digital LiDAR topography with 1-m-horizontal resolution when available (Oskin and Perg, 2006) and complemented with ASTER V003 30-m-horizontal resolution (NASA/METI/AIST/Japan Spacesystems and U.S./Japan ASTER Science Team, 2019) and ALOS 12-m-horizontal resolution (Tataku et al., 2014).We also study the drainages to understand their evolution and sediment transfer using the Hydrology Tools in ArcMap (ESRI). Variations in topography were studied using swath profiles constructed with the add-in SwathProfiler (Pérez-Peña et al., 2016) for ArcMap (ESRI).

3.1. Quaternary Alluvial Fan Surfaces

We identified the distinct Quaternary alluvial fan surfaces primarily through aerial imagery and detailed topographic analysis. We field checked the alluvial fan surfaces examining aspects of surface morphology and

their geomorphic positions. Alluvial fan surfaces were characterized by: i) the type of deposit and its soil development; ii) desert pavement formation, rock varnish development, clast rubification, swale and bar topography; and iii) stratigraphic relationships/morphostratigraphy and degree of incision.
We recognize three main alluvial surfaces: CR1 (youngest), CR2 and CR3 (oldest). The number of alluvial fan surfaces seems to be less than other neighboring areas.

3.2. Displacements of the alluvial fan surfaces

To estimate a long-term cumulative displacement along Camp Rock fault, geomorphic and geologic features were identified, selected and tentatively correlated cross the fault. Finding good piercing points to define fault offsets was challenging.

Common elements applied for strike-slips displacements are straight elements trending perpendicular or at a high angle to the fault and present on both sides of a fault. An adequate recognition of elements to be used as piercing points is crucial to estimate tectonic displacements. We recognized surface fan edges and sets of channels as being right laterally displaced in the study area and used those to estimate displacements of the CR2 and CR3 alluvial fan surfaces. The existence of surface processes such as erosion and sedimentation were taken into consideration for a miscorrelation and/or increased error in measurements.

Several assumptions were made for the displacement reconstruction:

1) for the purpose of simplification, the fault zone is a straight single fault trace.

2) the uphill pattern of drainage on the eastern side of the fault (eastern block) is directly correlated with the basins in the mountain. The main and larger channels are the main paths of sediment transportation down slope in the alluvial surfaces and their location is persistent through time. The main channels cross the fault zone into the western block during aseismic times. Once they are tectonically displaced, they became disconnected from the uphill channel (beheaded) and potentially preserved from erosion. Due to the continuation of lateral displacement through time, they can be connected to a different channel and re-occupied.

3) aerial imagery with color shows sediment with distinct colors, directly related with the bedrock in the mountain. Those sediments are transported down slope and areas with similar colors on both sides of the fault can be used to track lateral motion.

The displacements were reconstructed by matching geomorphic elements in remote sensing and measurements of cumulative displacements were done using LiDAR high resolution topography data when available or with ALOS digital topography. The lateral and vertical displacements were also calculated using the tool LaDiCAoz (Zielke and Arrowsmith, 2012; Zielke et al., 2015).

3.3. Sampling for dating

We aimed to date the intermediate and older surfaces (CR2 and CR3) because of the potential for large fault offset. We used TCN methods because the antiquity of the landforms meant that other dating methods such as radiocarbon and optically stimulated luminescence could not be readily applied. We sampled boulders and/or cobbles present at the surface for TCN surface exposure dating. We also collected sediment samples from a pit at equally spaced intervals for the initial 2 m depth from the surface for a TCN depth profile age. ^{10}Be was used for siliceous quartz-rich and ^{36}Cl for siliceous poor material. Boulders and cobbles were preferentially chosen if they: i) were quartz-rich (for ^{10}Be); ii) had well developed dark rock varnish; iii) had a dark varnish upside and orange to reddish undercoating, providing evidence that the clast has not been turnover; and iv) were at locations in a preserved and undisturbed area of the alluvial surface, reassuring the position as the original place of sedimentation.

About 32 quartz-rich surface cobbles were collected, and the upper 2 m of the surface deposits was sampled for a ^{10}Be depth profile for CR2 in the Camp Mine section. To help infer the TCN inheritance in the sediments, a sample from active channels sediment nearby was also collected. An additional 8 quartz-rich surface cobbles were sampled from CR2 in the Graben study area (Fig. 9).

We sampled 4 large boulders preserved in the top of a ridge on surface CR3 that is isolated from the mountain front by a linear ridge (Fig. 7k and 9). We used ^{36}Cl because the rocks contained little if any quartz. The boulders were selected due to their location in the alluvial fan surface, preservation from the mountain hill-slope deposits due to the linear ridge, and standing out from the surface, favoring an exposition to the cosmogenic rays. We did not do a depth profile in CR3 because the surface appeared to be very eroded and the soil had pedogenic calcic horizons which add much complexity to applying ^{36}Cl methods.

3.4. Laboratory work

Samples were processed in the Quaternary Geochronology Laboratories in the University of Cincinnati and measured in the Purdue Rare Isotope Measurement Laboratory (PRIMELab) in Purdue University. The preparation of samples ^{10}Be measurements require to isolate quartz and obtain BeO, following a sequence of mechanical and chemical steps, established by PRIMELab. Individual boulders and cobbles were crushed and pulverized, sieved and we set aside the 250–500 µm fraction for mineral separation and subsequent chemical preparation. The sediment for each of the depth profile samples was sieved into fractions of <250, 250–500, 500–1000 and >1000 µm particle size: we primarily used the 250–500 µm fraction when material was not sufficient, we added the 500–1000 µm was added. Samples for ^{10}Be were prepared for isolation of quartz grains. Samples were initially leached with an Aqua Regia solution (HCl/HNO_3) for 24 hours in order to remove carbonates, iron oxides coatings, phosphates and organics. The paramagnetic and magnetic mineral grains were removed through a Franz Magnetic Barrier Separator (LB-1). Samples were leached in a solution of 5% HF/HNO_3, in warm temperatures for 24 hours followed by another 24 hours in a 1% HF/HNO_3. Samples were frothed using a carbonated solution with CH_3COOH and Lauryl Amine to help remove mica and feldspar grains. Additional mineral separation aiming to isolate the quartz from remaining silicates was done through density separation using a lithium polytungstate (LST) solution with a density ~2.67 g/cm^3 in gravity separation funnels. The selected quartz purity was then tested in an ICP-OES (induced coupled plasma-optical emission spectrometry) for Al content: a threshold of 200 ppb of Al was used as reference. In the case that a sample still present a higher presence of Al, as a consequence of Al silicates inclusions in the quartz particles, the particle size is decrease by crushing it with zirconium grinding beads and then subject them to further 1% HF/HNO_3 leach to ensure the sample was primarily quartz and then re-tested. Once quartz is considered pure, sample was weighed in a PFA via, added ^{9}Be carrier and then dissolved in concentrated HF and HNO_3 and dried: several chemical blanks were simultaneously prepared to subtract the chemicals contribution. After, sample is transferred to a test tube and through solutions of NaOH and HCl we precipitate Fe, Ti removing them from the sample. Using solutions of HNO_3 and 30% NH_4OH and by evaluating the pH of the solution we control the precipitation of some species of Al to be removed from the sample and the final precipitation of a hydroxide of Al/Be. pH. We later elute the Be by passing the Al/Be hydroxide through several steps in ion exchange resin columns impregnated in several solutions. Finally, the Be hydroxide gel is precipitated with a solution with 10% EDTA and 30% NH_4OH, and pH ~9, dissolved with HNO_3, and dried in a dry bath. To obtain the BeO, the dry hydroxide is ignited in quartz vials placed in an oven at 900°C for 25 minutes. We mixed the resulting BeO of each sample with niobium powder (2:1 Nb:BeO ratio) and loaded each sample into a stainless-steel target for AMS analysis at the Purdue Rare Isotope Measurement Laboratory (PRIMELab). Measured ratios of ^{10}Be/^{9}Be and subsequent ages reported were corrected based on a chemical blank prepared alongside the samples.

The preparation of samples for ^{36}Cl measurements followed a sequence of mechanical and chemical steps, also established by PRIMELab: the silicate samples were crushed, pulverized, and sieved into < 250, 250 – 500, and > 500 µm particle size fractions. Approximately 100 g of the 250-500 µm fraction are subjected to a sequence of 3 leaches in a solution of 10% HNO_3 (TMG) for8 hours each. After being rinsed with deionized

water, and dried, chloride dilution spike carrier ($^{35}Cl/^{37}Cl$) was added to approximately 30 g of the leached sample in PTDE bottles, and then dissolved in HF and HNO_3 (TMG) solution. Several chemical blanks were simultaneously prepared to subtract the chemicals contribution and a direct measurement of the chloride dilution spike carrier ($^{35}Cl/^{37}Cl$) was also prepared.
After the sample is dissolved and decanted from residuum, $AgNO_3$is added to the solution to precipitate the Cl^- (and other anions, frequently SO_4^{-2}) as AgCl. The precipitate is then transferred to a test tube and through a solution of 3%$Ba(NO_3)_2$ and NH_4OH, sulfates are now removed from the sample and the precipitate is mainly AgCl. The Cl is finally eluted by passing the precipitate through ion exchange resin columns in several steps impregnated in several solutions and drying for approximately eight hours at 65° C. The isolated chlorine was loaded into copper cathodes for accelerator mass spectrometry at the Purdue University PRIME lab. Approximately 12 g of respectfully leached and not leached sample were sent to the Activation Laboratories Limited in Ancaster, Ontario, for geochemical analysis of major elements, uranium, thorium, and gamma emission spectrometry of boron and gadolinium, which are needed for the age calculation.

The boulders and cobbles ages were calculated using the online calculators: 1) for ^{10}Be CREP-Cosmic Ray Exposure program (https://crep.otelo.univ-lorraine.fr/#/) (Martin et al., 2017) and compared with results from CRONUS- Earth ^{10}Be exposure age calculator v.3 https://hess.ess.washington.edu/math/v3/v3_age_in.html) (Balco et al., 2008; Balco, 2017); and 2) for^{36}Cl exposure age calculator v.2 (http://cronus.cosmogenicnuclides.rocks/2.0/html/cl/) (Marrero et al., 2015). Ages were calculated using a topographic shield factor of 0.998 for all sites except CR2 Emerson site which was 0.999 and erosion is estimated to be zero in all sites except in CR3 where we assumed a value of 0.3mm/ka.

We model the cobbles ^{10}Be TCN ages assuming the production rate scheme of Lifton-Sato-Dunai (LSD; Lifton et al., 2014), the atmospheric model ERA40 (Uppala et al., 2005) and the geomagnetic database VDM (Lifton, 2016) and a production rate of 4.06±0.23 at/g/a. The boulders for ^{36}Cl ages were modeled assuming an erosion rate of 0.3 mm/ka, and a Lal (1991)/Stone (2000) time-dependent scaling model.

We use the individual ages from the boulders and cobbles to estimate the surface exposure age applying a probabilistic density function according with the methodology proposed by Zechar and Frankel (2009).

The ^{10}Be depth profile was modeled using a Matlab script for Monte Carlo simulations (Hidy and Goose, 2010, v1.2), using parameters that will be discussed in the results section.

3.5. Soil Characterization

Several abandoned mineral prospecting pits in the three surfaces allowed us to easily conduct preliminary investigations on the sediments and soils at several locations. We described the soil profiles for the different alluvial fan surfaces and used the soil descriptions to calculate their soil development index (SDI) using the methods of Harden (1982). We compare with the soil properties with the parent material and classified and estimate a profile development index (PDI) based in 8 parameters (rubification, texture, clay films, structure, consistence, melanization, paling, lightening), which provides a relative age based on regional soil chronosequences. The PDI age estimation can provide a large range of ages, since some of the soil proprieties reach a steady-state at different moments of the soil formation, staying the same through time.

3.6. Slip rate calculation

We calculated the slip rates using the measured displacements between geomorphic elements and the estimated TCN alluvial fan surface ages. The methods of Zechar and Frankel (2009) were used to determine slip-rate rates.

4. **Results**

4.1. Geological and Geomorphologic description of the study area

A swath topographic profile approximately perpendicular to the trend of the main active faults highlights the study area as a higher and narrow valley (Fig. 5). Interestingly, this valley is the highest elongated valley in the vicinity of Barstow and Lucerne Valley region.

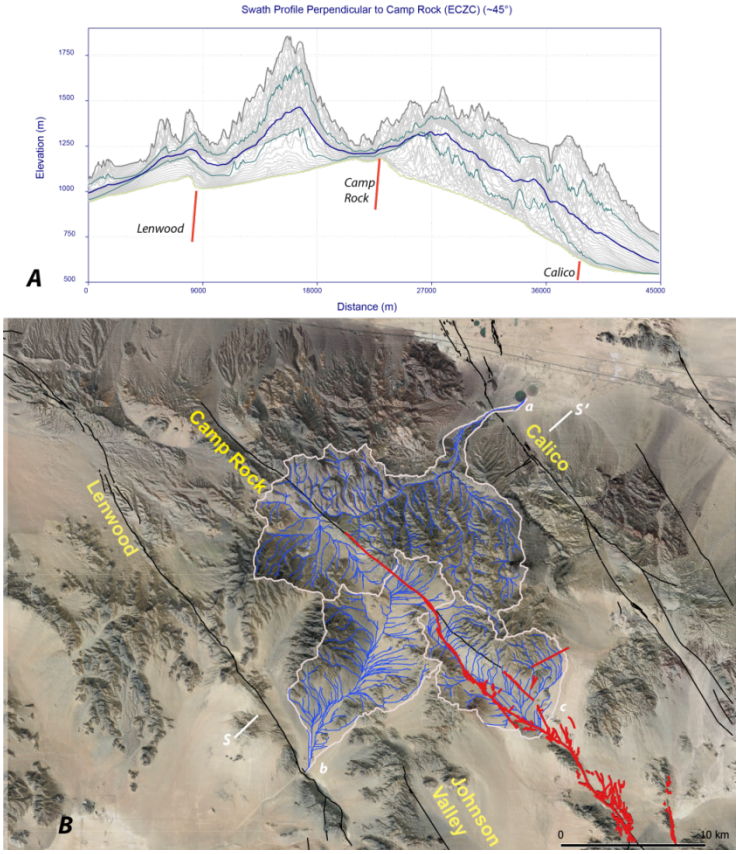

Figure 5. A - Swath profile along strike 45°, along S-S' location is in B; faults location are indicated, fault dip is not representative. B- Three main watersheds that are present in the study area: a- Kane Wash, b-SW flowing basin, c-SE flowing basin. Fault traces from the USGS Quaternary fault database and Satellite imagery over DEM (ALOS).

Three watersheds are present in the area: one corresponding to the upper Kane Wash basin, flowing northeastwards into the Troy Lake playa crossing the Calico fault; a second (no name) flowing towards SSW between Ord and East Ord Mountains towards the Lenwood fault and a third (no name) flowing southeastward, parallel to the graben in direction to the ephemeral Galway Lake (Fig.5). The Kane Wash has the largest area and higher elevation difference and, as such, has more incision and appears to be more active. Both Kane Wash and the graben catchment seem to be actively capturing the upper section of the central catchment, which seems to be only ephemerally active. This piracy conditioned a weak drainage activity in the Camp Mine fault area: the rills and creeks are essentially inactive, the loose sediment in the creek results from the local surfaces dismantling. The main channels uphill in the alluvial surfaces headward are smoothened, not sharply incised and seem to be inactive to ephemeral.

Further evidence of Kane Wash piracy and a poor drainage capacity of the central watershed are provided by the presence of two wind gaps in the Rodman Mountains (Fig. 6). These two wind gaps are a relic of a paleo drainage flowing from the Rodman Mountains southwards the Camp Mine fault area; their head wards were captured by the Kane Wash and eventually those locations are now draining northwards.

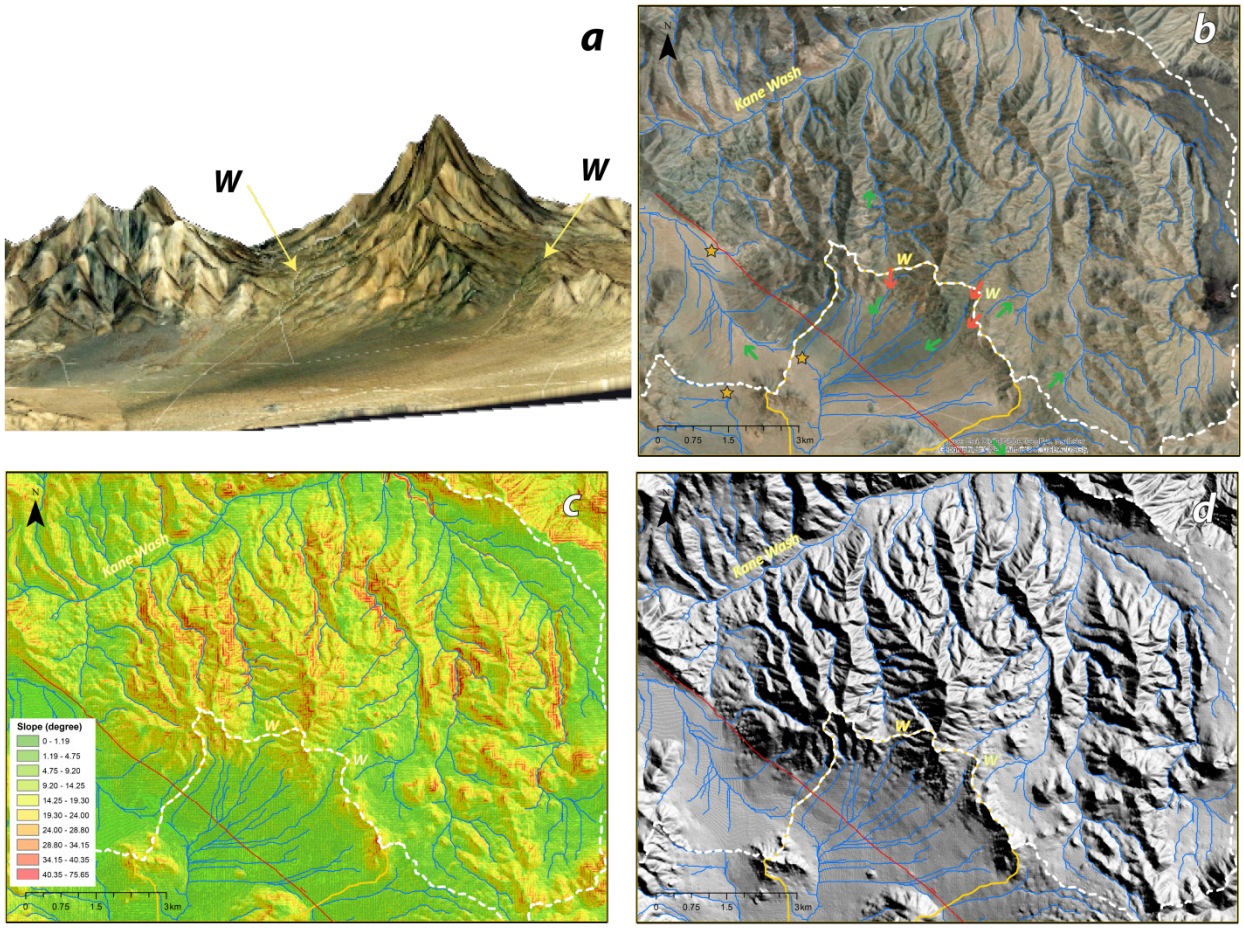

Figure 6. Interpretation of drainage piracy and wind gaps and in the Camp Mine fault section. a) 3D perspective from the mountain front, with the wind gaps (W); b) satellite image with the channels (in blue), and the delineation of the Kane Wash watershed (dashed white); delineation of central watershed (in yellow). Stars point the location of channels to be captured. Present direction of flow is marked by green arrows and paleo direction of flow is marked by red arrows. Camp Rock fault is the red trace; c) slope map; and d) shaded relief.

The mountain front has a similar shape for the two study areas: straight where the fault is located by the mountain slope and inflecting eastward acquiring a concave configuration when stepping away from the fault system.

At the Camp Mine study area, the mountain front has a low sinuosity namely across the head of the large fan, and the upland catchments have channels incised with steeper slopes (Fig. 5 and 6). However, while the active fault maintains its direction crossing the valley, the mountain front inflects eastward. The morphology then changes southwards, becoming more sinuous with channels increasingly less incised and edges less steep with smoother catchments divide. Along this part of the mountain front, two wind gaps are also identified (Fig. 6). A graben is formed where the Camp Rock fault steps to the right to the Emerson fault. The graben has a linear valley and the mountain fronts coincide with the faults. The western side (Emerson fault) has a lower sinuosity than the eastern side (the Camp Rock fault), probably due to a higher or recent activity of the Emerson. The Camp Rock fault ends here, and as such the eastern mountain front inflects eastwards becoming more sinuous with channels less incised and smoother morphology (Fig.5).

Along the Camp Rock fault, several relatively small size (100s m to ≤1 km wide) alluvial fans coalesce to form a bajada. At the north side of the bajada, a large (2 per 1 km) semi-circular alluvial cone, 100 m higher than the playa and 20 m higher than the bajada, outstands from all the other alluvial fans (Fig. 6). A basin with an area < 2 km^2 discharges to this larger fan through a canyon being its major sediments source. This basin can be subdivided in one ~300 m x ~650 m and another ~200m x ~500 m and both ~100 m elevation difference. The sum of this area of this source-basin is insufficient to have been the main sediment source through time. The Camp Rock fault trace is by the alluvial fan head and the alluvial fan main body is entirely in the western block. Since it is expected that the fan is right laterally displaced, it is likely than a source, or sources, for this alluvial fan are located in the eastern block farther to the southeast.

4.2. Alluvial fan surfaces, sediments and soils

4.2.1. Lower Surface CR1

The younger surface CR1 has a drainage pattern that can be characterized as braided, with several anastomosed channels, probably as result of avulsion and capture of channels. Some of the channels are ephemeral and likely to be occasionally flooded during exceptional rain events every few hundred years or so. Channels in the Camp Mine study area are a few meters wide and incised up to 0.5 m, but near the mountain front, can be 10 to 20 m wide and incised to depths of ~1 to 2 m, while in Graben study area, the channels can be 40 m wide, and incised to a depth of 3–4 m near the mountain front. The bars and swale morphology are generally well preserved, and the channel edges are being dismantled by clasts weathering and disaggregation and coarser clasts mobilized into the topographic low. The surface has little if any desert pavement and most surface cobbles are devoid of rock varnish (Fig. 7b). CR1 is inset into CR2 and CR3. Locally, thin layers of coarse sediments that we correlate with avulsion deposits, cover the intermediate surface CR2. Altogether this surface is interpreted as having little or no deposition during the past few 1000 years, due to the presence of a thin Av horizon.

The alluvial fan deposits are generally poorly cemented and poorly sorted, with particles size ranging from silt to cobble, generally sub angular to sub rounded. No stratification is clearly recognized, although changes in sedimentation are recognized. We interpret these CR1 deposits as debris flow deposits. A thin top layer with aeolian fine sand may be present at specific locations but is not widely present. The elevation of this surface decreases northwards in the Camp Mine study and southwards in Emerson section, similarly with the valley floor, and is generally inset into an older surface, frequently the surface CR2 in Camp Mine study area while in the Graben study area is generally incised in CR3.

The soil development is generally weakly to poorly develop and description can vary depending on location. Nevertheless the soil profile can be described as having a thin Av vesicular horizon ≤ 5 cm, a B horizon variable between 20 and 85 cm thick that includes a Bt horizon with a variable thickness between 25 and 50cm thick. Clasts within the soil have carbonate rinds that are a few mm thick and with carbonate precipitate filaments at several depths (plus gypsum), suggesting a calcic horizon stage I (Giles, 1961). Variations in the characteristics of soil development with changes in horizon thickness might be associated with different stages of deposition. Soil descriptions are consistent with previous descriptions in Camp Mine area (Shlemon, 1980; Kaneda and Rockwell, 2009). CR1 surface has variable colors from gray in the aerial imagery to different tones of brown which are directly related with the bedrock immediately near.

We correlate CR1 with the Q3 of latest Pleistocene/Early Holocene to Mid-Holocene age based on its surface characteristics and soil development (Bull, 1991; 1996). We consider that differences between Av and B thickness and variability in carbonate rinds can reflect a combination of Q3a and Q3b surfaces, which can be difficult to differentiate in our study area.

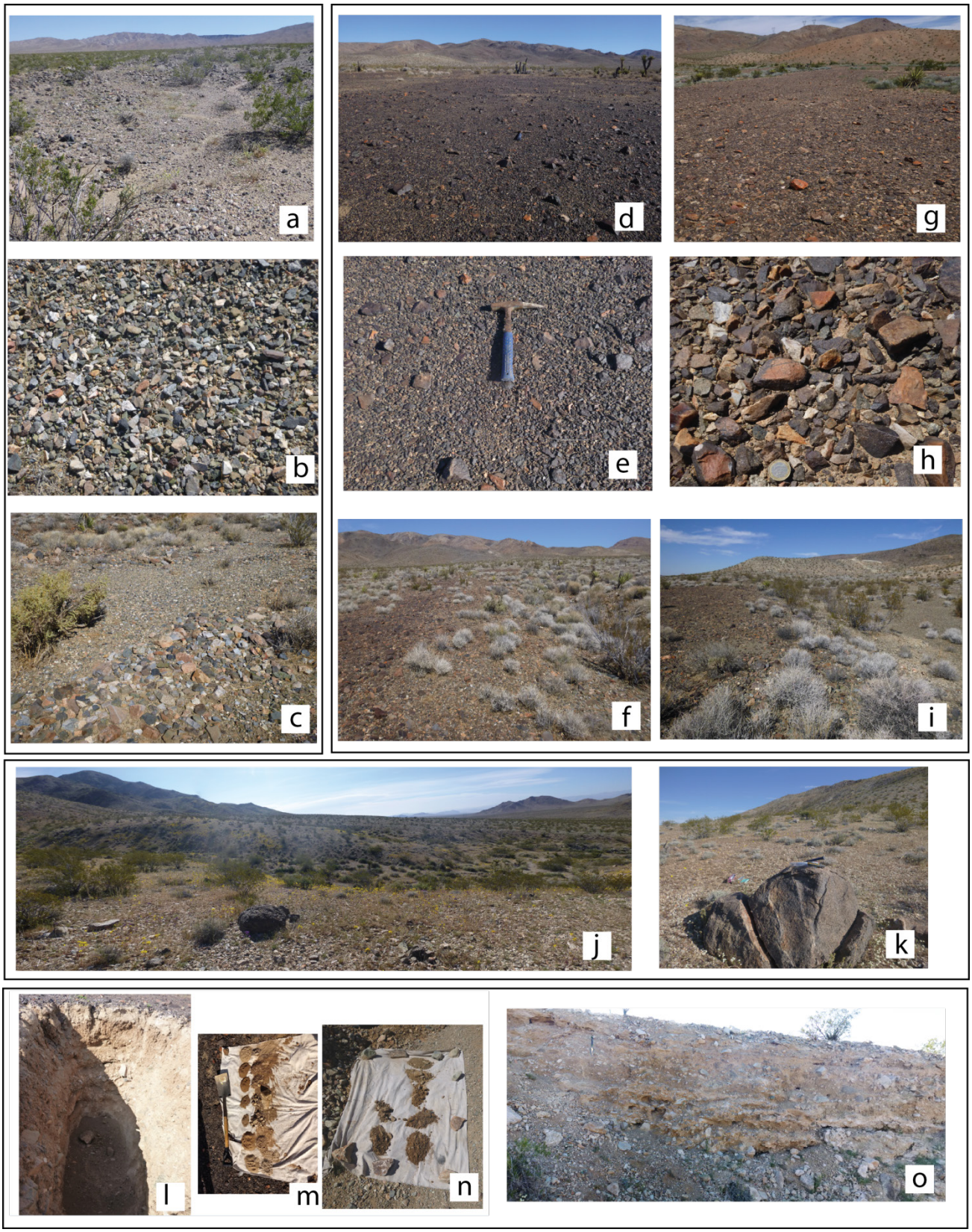

Figure 7. Several photos from CR1, CR2 and CR3 alluvial fan surfaces details. CR1 (a–c): a- general view of CR1 surface; b-clast interlocking in the surface; c- bar and swale morphology. CR2 (d–i): d-general view of

CR2 surface at Figure 7 cont. Camp Mine; e- Surface interlocking at Camp Mine; f- channel incision in CR2 and erosion; g- general view of surface CR2 at the graben study area; h- interlocking of surface CR2 in graben study area; i- fault scarp between CR2 and CR1 surfaces in Camp Mine study area. CR3 (j–k): j- general view of CR3 surface with one boulder; k- another view of CR3 with one of the boulders sampled. Soil (l–o): l- soil profile at the CM-pit: m and n- soil samples for CR2 Camp Mine and graben study areas; o- soil section at CR3, graben study area.

4.2.2. Intermediate Surface CR2

CR2 is the most ubiquitous surface along the Camp Mine study area and remnant in the southernmost Camp Rock, within the Graben study area. The surface is an alluvial fan with a moderate to well-developed desert pavement and with moderately dark to dark well-developed rock varnish. CR2 is preserved as remnants in the top of ridges when the channel incision is greater and is prominent as large patches well preserved where incision is lesser. These large patches are easily recognized in remote sensing, having lengths of >300 m and widths of 50 to 100 m, and are generally very sharp delineated by edges channels. The surface corresponds to a broad, flat surface, with no bar and swale topography (Figs. 5d, 5g). Unlike the other surfaces it has a continuous and well-developed desert pavement (80–100%) with interlocking surface clasts that have dark rock varnish and with strong rubification undercoating (Figs. 5e, 5h). Another characteristic on the surface is the absence of boulders nonetheless cobbles are largely distributed and are generally angular to sub-rounded and more frequent uphill. The alluvial fan deposits are poorly sorted and coarse grained, corresponding to layers of debris-flow occasionally interbedded with fanglomerates and channels, and the entire sequence is compacted unless is bioturbated.

The channel network is not very dense or developed, except closer to the Kane Wash where channel incision is greater, channel valleys can be up to 5 m deep, and the distance between the top of the valley walls being about 30 m. In most of the Camp Mine study area, the CR2 surface is ~1–2 m higher than the channels floor and the surface CR1, which is generally inset into it. Due to the capture of the Camp Mine drainage by the Kane Wash, incision is greater along the NW section of the large alluvial fan than in the SE side and the CR2 dark varnish surface remnants are sparse and less preserved (Fig. 7). We note that the distribution pattern of those CR2 remnants coincide with the cone shape suggesting that CR2 has developed equally through the entire alluvial fan. Locally, CR2 can be covered by sheets of debris flow, as a result of avulsion during some events.

We conducted a soil characterization in the new pit for ^{10}Be depth profile collection. Soil commonly has a 10-cm-thick gravelly loam vesicular Av horizon, a B horizon with thickness and sub-horizons variable that can include a Bt horizon with thickness of about 40 cm with common, discontinuous and moderately-thick clay films on ped faces and followed by a Btk of ~30–40 cm thickness, with carbonates filaments and coating in the base of the clasts, indicating calcic horizon stage I. At CM-Pit, a gravelly unit at ~90 cm depth possibly corresponds to a lithological contact with a fanglomerate or in alternative a possibly buried soil Btk with a calcic horizon stage II to III (Giles, 1961). Our observations are consistent with those of Shlemon (1980) in his trench T2 that is located ~800 m to the east of CM-pit, and with the soil descriptions by Kaneda and Rockwell (2009). Detailed soil descriptions are provided in Table 1. The PDI calculated for the CR2 surface at Camp Mine is 27 indicating a relative age of 295 ka with an upper and lower bound of 520 and 70 ka, respectively. While for the Emerson section the PDI is 31 indicating a slightly older age of 494 ka with an upper and lower bound of 870 and 118 ka, respectively (Fig.9).

This CR2 surface is mapped partially as Qoa (Older Alluvium) in Dibble (1964) and as Qia (Intermediate Fan Alluvial deposits) in Phelps et al. (2011), assumed to be late to mid Pleistocene in age and corresponding to the Q2 terraces of Bull (1991) that spam from ~50 to 500 ka. Different degrees of incision are present, and may be useful to differentiate relative ages and sub-units.

Table 1. Soil descriptions for surfaces CR2 and CR3.

Horizon	Depth (cm)	Boundary	Color		Texture Class	Clay [%]	Structure	Clay Films	Consistence			Reaction	Other Notes
			Dry	Moist					Dry	Wet			
										Stickiness	Plasticity		
CR2, CM-pit PDI = 38 including buried horizons, PDI=27 not including buried horizons													
Desert Pavement - near complete interlocking (80-100% of surface) w/ strong varnish													
Avk	0-10	AS	10YR 5/4	10YR 3/4	gr l	18	2tk pl→ 3vf sbk	--	SH	SO	PO	VE matrix	Vesicular pores - using "v" subscript notation to denote
Bt1	10-26	CS	7.5YR 4/4	7.5YR 3/4	vgr sicl	50	3m sbk	c, p, f, pf	FI	MS	VP	--	
Bt2	26-50	CS	7.5YR 4/6	7.5YR 3/4	vgr sic	42	3m sbk	m, c, d, pf	FR	MS	VP	--	
2Btk1	50-60	CS	10YR 6/4	10YR 4/4	xgr sc	45	2m sbk	c, d, d, pf	FI	SS	MP	ST masses and bottom of gravels	Stage I; lithologic discontinuity
2Btk2	60-88	CS	10YR 6/4	10YR 4/4	xgr sc	42	2m sbk	f, p, f, pf	VFI	SS	MP	ST masses and bottom of gravels	Stage I; lithologic discontinuity
2Btkb1*	88-100	CS	7.5YR 5/6	7.5YR 4/6	gr sc	50	2co sbk	f, p, f, pf	FR	SS	MP	VE masses throughout matrix	Stage II; lithologic discontinuity and/or buried horizon?
2Btkb2*	100-130		7.5YR 6/4	7.5YR 5/4	vgr scl*	38	2co sbk	f, p, f, pf	FI	SS	MP	VE masses throughout matrix	Stage II - bordering on Stage III; lithologic discontinuity and/or buried horizon?
*buried? - change in color suggests buried horizons *bordering on sc													
CR2- Emerson PDI =31													
Desert Pavement - near complete interlocking (80-100% of surface) w/ strong varnish													
Avk	0-10	AS	10YR 5/4	10YR 4/4	vgr cl	30	2tk pl→3co sbk	--	SH	SS	SP	SL matrix	Vesicular pores
Bk1	10-40	CS	7.5YR 5/4	7.5YR 3/4	vgr c	40	2m sbk	--	FR	SS	MP	SL patches/bottom of gravels	Stage I carbonates
Btk1	40-70	CS	7.5YR 4/6	7.5YR 3/4	vgr sc	45	2f sbk	m, c, p, pf	FR	SS	MP	ST filaments/bottom of gravels	Stage I carbonates
Btk2	70-94	CS	7.5YR 4/6	7.5YR 3/4	vgr scl	25	2f pr	f, p, f, pf	FR	SS	MP	ST filaments/bottom of gravels	Stage I carbonates
2BCk	94-113	CS	7.5YR 6/4	7.5YR 4/4	vgr cos	5	1f sbk	--	LO	SO	PO	VE masses/bottom of gravels	Stage I-II carbonates; 2-3 mm coatings on bottom of gravels; lithologic discontinuity
2CBk	113-120		10YR 6/4	10YR 4/4	vgr cos	5	1f pr	--	FR	SO	PO	VE patches and matrix	Stage 1 carbonates; lithologic discontinuity
CR3-Emerson PDI=40													
Av	0-3	AS	7.5YR 4/6	10YR 4/4	vgr cl	30	2tk pl→ 3co sbk	--	FR	SS	SP	--	Vesicular pores
A	3-10	CS	7.5YR 4/6	7.5YR 3/4	vgr c	40	2m sbk	--	FR	SS	MP	--	
Bt	10-42	CS	5YR→2.5YR 5/6	7.5YR 3/4	vgr sc	45	2f sbk	m, c, p, pf	FI	SS	MP	--	
Btk	42-70	AS	5YR 4/6	7.5YR 3/4	vgr scl	25	2f pr	c, d, d, pf	FR	SS	MP	SL filaments	Stage 1 filaments in matrix
Bkkm	70-89	CW	10YR 8/1	7.5YR 4/4	vgr cos	5	1f sbk	--	EH	SO	PO	VE	Stage IV to V; 0.5-1 cm thick laminar cap at bdry; multiple layers of cemented laminar caps to 89 cm
Bkk	89-120		5YR 8/1	10YR 4/4	vgr cos	5	1f pr	--	VH	SO	PO	VE	Stage III; weakly cemented in areas;

4.2.3. Upper Surface CR3

Surface CR3 is only present in the graben along the southern Camp Rock fault trace (Fig.6). The alluvial fan surface is present along most of the eastern mountain front and their heads are generally by the mountain front where the fault is located. The fault zone along this mountain front is frequently composed by two main parallel faults, vertical and 20–30 m apart. This surface is completely smoothened, with no preservation of swale and bar morphology. Channel incision is greater in the northern and central graben: channels incision is 4 to 9 m deep, and the valleys tops are up to 150 m wide. The surface is generally eroded, and remnants of

desert pavement are preserved at some locations. Rock varnish on the clasts is weathering away, except for the clasts in the top of the ridges. There are a few boulders preserved on CR3.

The soil for CR3 surface is characterized by an upper vesicular Av sub-horizon very thin (0–3 cm), and a thin argilic soil Bt (~30 cm) that is absent in many places. This Bt, evolves to a Btk rich in stage I filaments strongly effervescent in matrix and with clasts with Ca coating in their bases. A Bkkm, at about 70–90 cm depth indicates a stage IV to V (Gile et al., 1981). A laminar cap in top of a Bkk stage III calcic horizon is widespread in this CR3 surface, well developed and weakly cemented in certain areas. This Bkk horizon is frequently exposed, due to the ongoing erosion of the upper soil horizons in CR3. Locally, in the vicinity of larger channels, smaller surfaces are inset in CR3, however without a significant expression or being displaced by the fault. The PDI calculated for this surface is 40, providing a relative age of 956 ka with a lower and an upper end of 229 and 1650 ka respectively.

This surface is mapped as the same alluvial unit that CR2 in both existing geological maps. CR2 is likely the same age as the Q2 surface of Bull (1991).

4.3. Surface deformation and displacements

During the Landers rupture, a horizontal displacement up to 1 m along the Camp Mine section occurred (Sieh, 1996) added to 2 (or 3) Holocene paleo-events (Rockwell et al., 2000) indicates that horizontal cumulative displacement of CR1 surface is expected. Aerial imagery and field survey corroborate evidence of right laterally deflected channels along the fault trace; however, channels deflecting left laterally were also recognized, which raised questions about the nature of the channel geometry. We chose not to quantify a cumulative horizontal displacement for CR1 surface due to:1) a lack of identifying unequivocal displaced linear features with precise piercing points to measure displacement: and 2) observation of other linear features that cross the fault zone without having horizontal deformation. Vertical deformation assumed to be Holocene is observed locally as surface folding and scarps generally facing NE with heights ≥0.5 m. The Landers vertical slip was generally <20 cm with the exception of an anomalous location where it could had been ≤60 cm (Kaneda and Rockwell, 2009).

Deformation in CR2 surface, is expressed by scarps generally facing NE along the Camp Mine fault trace, with heights as much as 1 m provides evidence for vertical deformation (Fig. 5i). These scarps are likely to represent cumulative vertical displacements, however in some cases they can also be generated by lateral displacement of pre-existing morphologies, as elevated alluvial fan surfaces. Patches of the CR2 surface with similar characteristics are distributed and some end abruptly along the Camp Rock fault, indicating that are likely to be displaced: the majority of them in the eastern side of the fault are located southward while the ones west of the fault trace are northwards, corroborating a cumulative right lateral displacement (Figs. 8 and 9). Further corroboration of lateral displacements is provided by correlation of alluvial fans edges and preserved paleo channels.

The heads of the CR3 alluvial fan surfaces are generally right laterally displaced, promoting the existence of linear ridges, some of them acting as shutter ridges. No vertical deformation is observed directly in the surfaces, or abrupt changes in the surface slopes. Towards the northern graben, where the Emerson fault merges with the Camp Rock fault, channel incision is higher and evidence of a fluvial terrace 2 m higher than the active channel indicates that the channels are adjusting to a change of base level, probably due to an event prior to Landers. Bull (1996) made a similar observation for Emerson fault, which an ephemeral stream had adjusted to a lowering of the pull-apart basin probably during a Holocene event prior to Landers. Long-term cumulative lateral displacement is inferred through correlation of alluvial fans and channels and short-term displacement is also recognized by channels right laterally deflected or displaced up to 10 m, which can be indicative of 2–3 earthquakes during the Holocene prior to the Landers earthquake. The Landers earthquake in Graben study area ruptured only in the southern section, which is largely now within military base.

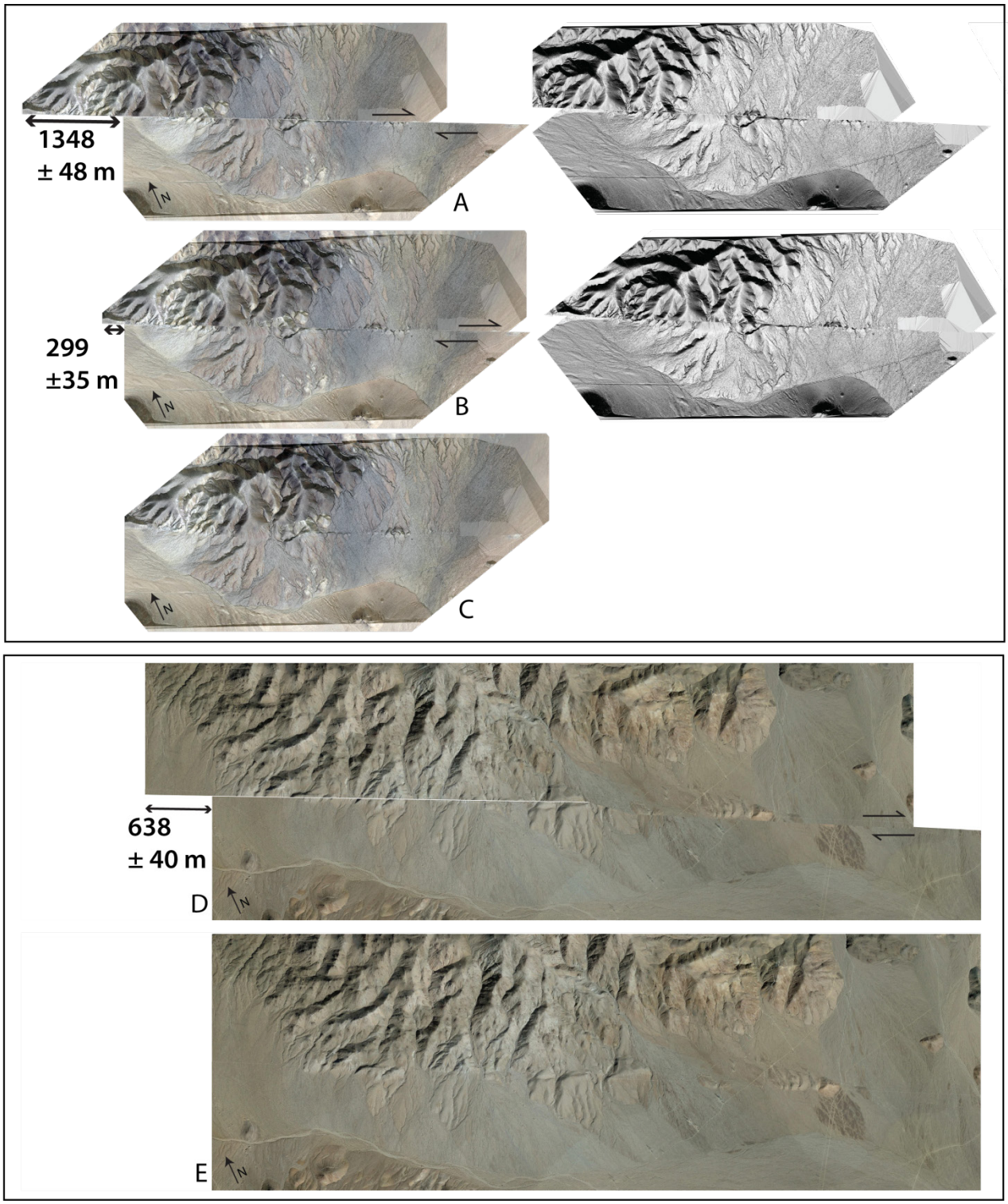

Figure 8. Reconstructions of the displacements for Camp Rock fault along Camp Mine(A-C) and the graben (D-E) study areas. along the, corresponding to the area covered by Lidar. Camp Mine imagery corresponds to satellite imagery overlapping 1-m-resolution DEM Shaded relief model and graben is Google Earth imagery. A-reconstruction for the Camp Mine showing a displacement of 1348 ± 48 m; B- reconstruction for the Camp Mine showing a displacement of 299 ± 35 m; C- present day. D- reconstruction for the graben study area showing a displacement of 638 ± 40 m; E- present day.

We present different scenarios for reconstructing the offset alluvial fans at the Camp Mine study area. Firstly, displacement of 299±35 m is determined supported by a correlation between CR2 surface patches, alignment of a principal alluvial fan lobe in the larger alluvial fan body, with a larger basin, however we note than this lobe is younger than surface CR2 (red arrows). The eastern side of the larger alluvial fan body, rich in light color sediments, is a match with be light color bedrock. The southernmost CR2 surfaces uphill are visibly offset by the fault, however in this reconstruction, we were unable to find correlative surfaces across the fault trace. This reconstruction corresponds possibly to an offset occurred after the generation of the light color lobe, younger than CR2 (Fig.8).

A displacement of 1384±48 m is supported by the majority of the CR2 surfaces being correlated in both sides of the fault. The pattern of the dark surfaces is a match in most of the existent surfaces in both fault blocks. The main channels pattern uphill correlates with the paleo-drainage pattern downhill, suggesting a common drainage pattern. Light color alluvial fans sediments in the northern side of the western block, correlate well with light color bedrock lithology. This light color bedrock is monzonite, and is locally limited by an ESE-WNW not active and minor fault. Furthermore, this reconstruction allows connecting an anomalous high topography that outstands as a CR2 with a higher slope. This feature, been interpreted as evidence of local vertical deformation, however this feature can also correspond to a higher alluvial fan that was displaced. Finally, the large alluvial fan with a cone shape may be correlated with a larger basin uphill, presently captured and not active towards the Camp Mine mountain front (Fig. 5 and 9). Evidence for the existence of these sources is the wind gaps.

A clearer displacement reconstruction is undertaken for the Emerson section, based in the re-alignment of several CR3 alluvial fans with were beheaded, allows to estimate a cumulative displacement for CR3 of 638±40 m (Fig. 16). No reliable correlation for the CR2 surface was possible to establish, due to the remaining surface being inside a military perimeter.

Due to the overall alluvial fan smoothened morphology, with is characterized by moderate incision, frequently <1 m, the resolution of available digital topography, we found that applying slope and surface roughness analysis is frequently not adequate to differentiate the alluvial fan surfaces, and apply to estimate displacements

4.4. Geochronology results and correlation with regional surfaces

4.4.1. CR2 geochronology results

Most of the rocks outcropping in the Camp Mine area are siliceous, however they are aphanitic felsic-rich volcanic rock. Cobbles quartz-rich likely derived from quartz veins are present, found only along certain CR-2 patches. We interpreted their location in the fan, as related with the bedrock original location and drainage pattern. These cobbles were present mainly in the southern edge of the surfaces located west of the fault, while east of the fault (up-fan) the cobbles were found along the edges of the patches incised by the main channels flowing from the mountain. At the Emerson section the cobbles quartz-rich are widespread in CR2.

The majority of the quartz samples being veins were rich in mineralization. During the physical and chemical preparation to isolate the quartz particles for the Be extraction, we found that the quartz had mineral inclusions rich in Aluminum, most likely feldspar and other silicates such as kyanite and/or sillimanite. We verified the purity of quartz through ICP-OES chemical analyses to measure the amount of Al and other cations. We used a threshold of 200 ppb Al to accept quartz for Be extraction. This required further physical and chemical preparation to purify the quartz, which eventually decrease the amount of available quartz and limited the usage of some of samples. All data referring to the TCN samples is presented in Table 2.
We obtained results at 4 locations: two in CR2 surface at Camp Mine study area 1) in the middle fan/bajada west of the fault; 2) in the middle/upper fan/bajada east of the fault: two others in the Graben study area 3) in a CR2 remnant east of the fault, near the fault termination and 4) in an older CR3 fan surface (Fig. 9).

In the CR2 patch located west of the fault in Camp Mine study area, we obtained ages for 6 cobbles, ranging from 165 to 333 ka. We consider the youngest cobble to be an outline and with the other 5 cobbles we estimate an age of $278^{+80}/_{-78}$ ka for this site. We also note that the cobbles cluster in two groups, one ~220 ka and the other ~300 ka.
For the other two locations, we were able to obtain 2 ages for each site, and as such we calculated a mean value to estimate the surface age. We obtained two ages of 115 ±6 and 194±11 ka that provides a mean age of 155±9 ka for the second location at Camp Mine study area, which is much younger than the age inferred for the other CR2 patch in the Camp Mine study area. The main CR2 patch at Graben study area provides two ages of 230±14 and 322±19 ka, providing a mean age of 276±17 ka, which is very similar with the age of the western CR2 patch. Regarding the sample collected from the active channel aiming to estimate inheritance, we estimate an age of 134±23 ka, which however we are not interpreting as a realistic age for the channel.

We were able to measure 3 samples at 45, 85 and 145 cm for the depth profile, being the 85 cm one a poor quality one, with high error. The ^{10}Be concentration with depth does not show the expected exponential decrease with depth, which argues for the burial of a surface previously exposed, as also suggested by the soil profile description. We tentatively modeled the depth profile with the available data, assuming an erosion range from 0 to 0.4 mm/a, a minimum and a maximum age of 100 and 400 ka, and erosion threshold up to 50 cm. We collected a sediment sample from the active channel to estimate the sediment inheritance, which we estimate to be high in the range of 1,000000. However, unless we choose a high chi-square or sigma-value we were unable to obtain Monte Carlo solutions. We chose not to accept those results, since they had a low confidence level and may affect significantly our results.

Ages from the surface CR2 at two locations are consistent between them, and in addition are consistent with the ages estimated from the PDI inferred through the soils. These results strongly agree with the view that these CR2 surfaces are synchronous and have a widespread expression in our study area. The patch in Camp Mine study area east of the fault provided an age of 155±9 ka, which is very close to the younger outliner, 165±10 ka. These younger age cobbles are located closer to the surface edge and proximal to the channel, and that this younger cobble may be associated with avulsion deposits. We interpret these results as being consistent and evidence of a younger deposition that may partially cover surface CR2, and not representative of a CR2 age.

The Q2b surface of Bull (1991, 1996) has been argued to have formed during the last interglacial at ~125 ka (MIS 5e), however, our ages suggest it is older. CR2 surface is very similar in terms of: i) desert pavement and rock varnish development on clasts; and ii) soil development with an alluvial fan surface in the eastern side of the Newberry Mountains, described by Xie et al. (2018) that has a ^{10}Be age of 346±24 ka. Characterization of soil and calculation of a PDI of 26 provided an age equivalent of 250 ka with an upper and lower bound of 425 and 60 ka, respectively.

4.4.2. CR3 geochronology results
We determined ^{36}Cl TCN ages for 4 boulders and then using those we estimated CR3 a PDF surface exposure age. We obtained ages ranging from 284 to 470 ka and we estimate a PDF surface age for CR3 is $351^{+352}/_{-233}$ ka assuming 2σ or $351^{+157}/_{-123}$ ka assuming 1σ confidence (Fig. 9). These results also are within the range of the PDI estimation (956 ka with a lower and an upper end of 229 and 1650 ka, respectively). We prefer to use the 1σ for our estimates since it constrains the error range associated with it. These results are also consistent with the PDI estimated for the surface that estimates a lower bound of 229 ka and an upper bound of 1650 ka.

This surface corresponds to the Q2a descriptions of Bull (1991), assumed to be ≥ 400–500 ka (in comparison with Colorado region) and was not previously dated with geochronology methods in the region.

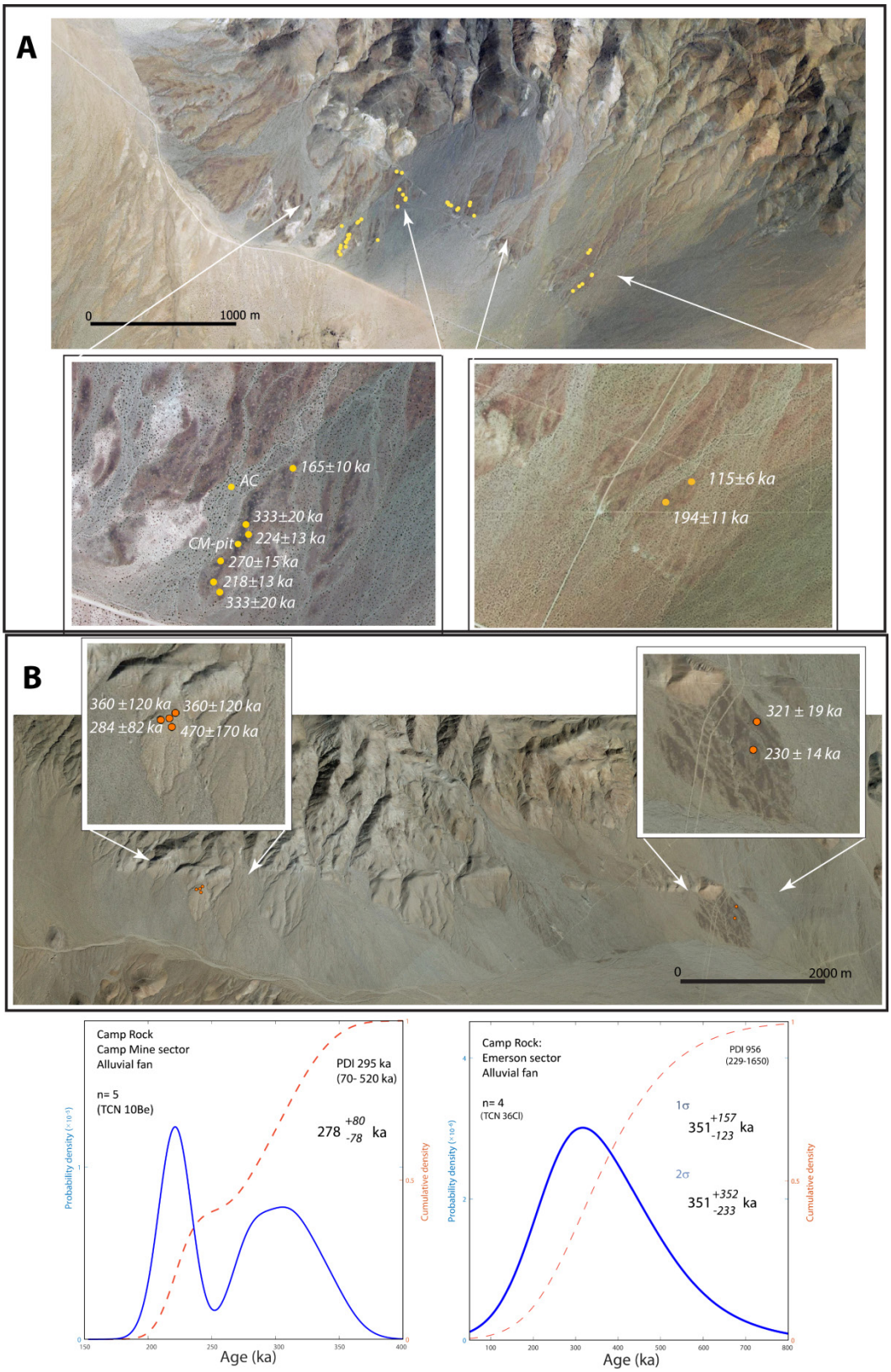

Figure 9. Location of TCN samples and PDF age surface calculation for CR2 and CR3. A- Location of samples and ^{10}Be TCN results obtained for CR2 at Camp Mine study area. B- Location of samples and ^{10}Be and ^{36}Cl TCN results obtained for CR3 and CR2.

Table 2. Summary of ^{10}Be and ^{36}Cl Sample Data

Sample[1]	Latitude (°N)	Longitude (°W)	Surface Elevation (m)	Quartz Mass[2] (g)	^{9}Be Carrier Mass[3] (g)	Corrected ^{10}Be/^{9}Be[4,5] x 10^{-12}	^{10}Be Concentration[5,6] (atoms/g SiO_2 x 10^6)	Age[3,5,7] (LSD[8]) (ka)	
Pit-45	34.679331	118.075	1211	3.4091	0.3320	1.8721	1.274	1.8721	1.274
Pit-60	34.679331	118.075	1211						
Pit-85	34.679331	118.075	1211	12.5700	0.3165	1.12641	1.982	1.12641	1.982
Pit-110	34.679331	118.075	1211						
Pit-148	34.679331	118.075	1211	3.7679	0.3402	0.50531	3.189	0.50531	3.189
CR-AC	34.679488	116.720799	1199	6.1963	0.3491	0.27794	1.094	0.27794	1.094
CM-01	34.678572	-116.720841	1204	17.5898	0.3321	2.00592	2.647	2.00592	2.647
CM-02	34.678752	-116.720972	1203	17.4183	0.3342	1.3255	1.777	1.3255	1.777
CM-04	34.679588	-116.720225	1202	18.1787	0.3424	1.864	2.454	1.864	2.454
CM-06	34.679122	-116.72082	1198	20.1371	0.3509	1.82848	2.227	1.82848	2.227
CM-11	34.679763	-116.720278	1200	18.868	0.3561	1.37449	1.813	1.37449	1.813
CM-14	34.68075	-116.719274	1206	17.1234	0.3744	0.874183	1.336	0.874183	1.336
CM-30	34.676562	-116.702960	1230	3.958	0.3507	0.176831	1.609	.0176831	1.609
CM-32	34.67724	-116.70203	1235	22.7162	0.3209	0.17883	9.630	.017883	9.630
CR-S5	34.610333	-116.61674	1080	20.3492	0.378	0.129681	1.684	0.129681	1.684
CR-S8	34.60995	-116.617596	1077	18.256	0.3487	0.170216	2.272	0.170216	2.272

Sample[1]	Latitude (°N)	Longitude (°W)	Elevation (m.a.s.l.)	Boulder Size Long Axis/Height (cm)	Sample[2] (g)	^{35}Cl Carrier[3] (g)	Cl (ppm)	^{36}Cl Concentration (atoms/g ^{36}Cl x 10^6)[5,6,]	Exposure Age (ST) ± Uncertainty (ka)	Exposure Age (LSD) ± External Error (ka)
CR-S1	34.6355	116.65962	876		31.4278	1.0641	1008.00	24.185±1.5	470 ± 170	430±160
CR-S2	34.63601	116.65919	876	0	31.0510	1.0534	830.95	16.959±1.5	360 ± 120	300±100
CR-S3	34.636439	116.659272	875		31.1624	1.1201	599.10	13.119±0.8	360 ± 120	300±100
CR-S4	34.636401	116.659725	876	100/100	31.4604	1.1498	1294.78	22.154±1.8	274 ± 82	256 ± 71

[1]All calculations include a Topographic shielding factor calculated using CHRONUS tool online (https://hess.ess.washington.edu/) of 0.99, except for the CR-S1 to CR-S5 and CR-S8 that had 0.98.
[2] A density of 2.65 g cm^{-3} was applied to all calculations.
[3] The ^{9}Be and ^{35}Cl carrier had a concentration of 1045.9 ppm and 1.0069 ppm respectively.
[4] Isotope ratios were normalized to ^{10}Be standards prepared by Nishiizumi et al. (2007) with a value of 2.85 x 10^{12} and using a ^{10}Be half-life of 1.36 x 10^6 years.
[5] Uncertainties are reported at the 1σ confidence level.
[6]Propogated uncertainties include error in the blank, carrier mass (1%), and counting statistics.
[7]Propogated errors in the model ages include a 6% uncertainty in the production rate of ^{10}Be and a 4% uncertainty in the ^{10}Be decay constant.
[8]Lifton-Sato-Dunai time-dependent (LSD) scaling model ± total uncertainty calculated on CREp online calculator (https://crep.otelo.univ-lorraine.fr/#/).
[9]Lal and Stone time independent (ST) scaling model calculated on CHRONUS v.2 online calculator (http://cronus.cosmogenicnuclides.rocks/2.0/html/cl/).
[10]Lifton-Sato- Dunai time-dependent (SF) scaling model calculated on CHRONUS v.2 online calculator.

4.5. Slip-rates

Regarding the Camp Mine section, and considering a CR2 age of $279^{+80}/_{-78}$ ka we estimate a slip rate of $1.1^{+0.3}/_{-0.2}$ mm/a for a displacement of 299±35 m or a slip-rate of $4.9^{+1.9}/_{-1.1}$ mm/a if we assume a displacement of 1384±48 m.

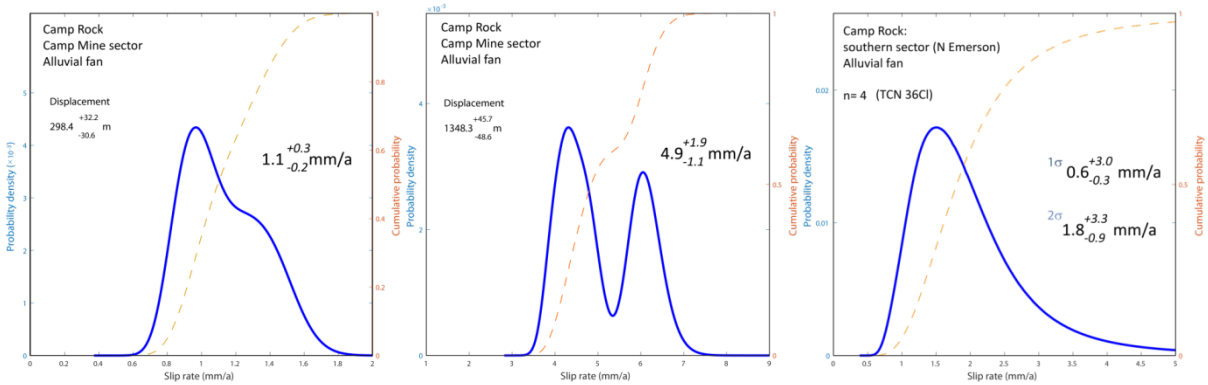

Figure 10. Slip-rate PDF calculations for Camp Mine study area and Graben (southern sector).

Our estimated slip-rate for the Emerson section, based on the displacement of CR1 surface is $0.6^{+3}/_{-0.3}$ mm/a assuming the TCN ^{36}Cl age of $351^{+157}/_{-123}$ ka.

5. Discussion

5.1. Quaternary paleoenvironmental change and landscape evolution implications

The valley where our studies were conducted corresponds to a preserved and isolated valley, higher in elevation than most of other linear valleys controlled by active structures in the region. We also show evidence for a change in the drainage system that was captured and as such favoring a decreased of the amount of sediments carried into the valley. The lack of an active drainage system also favored the preservation of the alluvial deposits and morphologies, formed before the capture of the drainage.

The combination of the valley conditions may be unique within the region, and it is possible that the aggradation and incision periods associated to the surfaces here may not be representative of alluvial fan surfaces at lower elevations and along other mountain fronts. The number of surfaces here seems to be fewer that at other locations. Shepard et al. (2018) found cyclicality in soil chronosequences that suggest a correlation with orbitally driven climatic changes. The soils are predominantly preserved during periods of relatively low rates of climate change, following periods of rapid climate shifts like during glacial-to-interglacial cycles, where aggradation and alluvial fan generation are favored. Evidence for this cyclicality may be present in our study area, where pulses of deposition during climatic transitions generated the alluvial fan deposits where soils developed during and are preserved. The lake and alluvial fan records in the Mojave reflect periods of rapid climate change (Reheis et al., 2012).

Miller et al. (2015) indicates regional three main pulses of fan aggradation for the Mojave from ~930–500 ka, ~253–125 ka and ~105–20 ka. Several buried soils in a Manix Lake core were recognized for ~450 ka, ~420–400 ka, ~230 ka, ~150, ~130 ka and ~40 ka (Reheis et al., (2012).

Our results estimate a TCN ^{10}Be surface exposure age for CR2 older than the predicted last interglacial age and suggests an older surface generation. Our interpretation is that the alluvial fan surface may potentially correspond to the penultimate interglacial MIS7 (~190–250 ka) in the case that the cobbles have an inherited TCN cosmogenic overprint or the alluvial fan aggradation may even occurred during a period lasting from MIS8.5 (~280–290 ka, a warm glacial) to the MIS9 (290–330 ka). Our preferred option is that the alluvial fan aggradation is associated to a rapid climate change which seemed to be associated to the period MIS 9 to MIS

8.5. However, a cluster of younger cobbles and a younger outline were found in CR2, with similar ages, providing an age range of 155–165 ka, which can be associated with the MIS6. Evidence for dry and warm climate ~186–192 ka followed by a cooler and weather climate ~128–186 ka was recognized in a Death Valley core (Lowenstein et al., 1999) and may indicate a climate transition.

Our interpretation is that the cobbles with 155–165 ka are testimonies of deposits that partially covered or even buried locally the CR2. The argument for this reasoning is that these cobbles were found in the vicinity of the surface edges and in areas easily exposed to the active channels. If these are evidence of sediment flux out of the Rodman Mountains it suggests that the capture of the mountain drainages might have occurred after155–165 ka. The absence of an active drainage with stream power to form new deposits may justify the absence of MIS 5 deposits and the preservation of older deposits and soil.

We estimated an age of 134±23 ka for the sediment collected from the "active" channel in CR1 aimed to estimate inheritance. However, we do not advocate that the CR1surface has this age due to the absence of soil or any type of coating in the sediment collected, and overall preservation of bar and swale morphology. We identified that the channels are being fed with material resulting from the dismantling of nearby deposits, and as such the higher age reflects inheritance.

Our study of CR2 is consistent with Q2b topography and soil-profile horizons of Bull (1996), despite an older age. We suggest that the regional Q2b geomorphic surface might have sub-units corresponding to periods of aggradation that were diachronic during a period of time that lasted since the last to the antepenultimate interglacial. We assume that the obtained ^{36}Cl TCN surface exposure age for CR3, may correspond to MIS 11 (or even 12) and is likely to be a minimum surface exposure age, due to the prevailing erosion in the surface. We correlate our surface and soil observations with the Q2a geomorphic surface from Bull (1991, 1996).

5.2. Estimation of geological slip-rates

A general concern in a geological slip rates database are the intrinsic uncertainties, a problem that has been recognized and addressed by several studies (Bird, 2007; Zechar and Frankel, 2009; Zielke et al., 2015; Resor et al., 2018). Since geological slip rates correspond to ratios between the displacement of a geologic or geomorphic marker and the time inferred for that translation, uncertainties will relate primarily with limitations on displacements measurements and/or the geochronology processes. In our study area, surface processes seemed to have very low rates, which could favor preservation of evidences for long term displacement. The specific constrains caused by surface processes in the measurement of displacements along strike-slip active faulting is recognized in several active tectonic studies (i.e. Klinger et al., 2011; Zielke et al., 2015), generally assuming the effects of surface processes over a few number of earthquakes, and within a time span up to some tens of ka. In our study, it is likely that multiple earthquake cycles (possibly ≥100) since the formation of our surfaces several hundreds of thousands of year ago.

Further considerations related to fault geometry should also be taken into account as single site geologic measurements may not be representative for a given fault segment (Resor, 2018), especially if off-fault deformation or a surface slip deficit are demonstrable. Several studies (geologic, geodetic, and remote sensing) have demonstrated the worldwide existence of OFD with variable widths and different magnitudes of strain accommodation (e.g. Gold et al., 2015; Milliner et al., 2015; Rockwell et al., 2002; Shelef and Oskin, 2010; Zinke et al., 2014). Specifically, for the MECSZ, OFD has a significant role accommodating an average 40±23% of the total strain (Herbert et al., 2014b) and, in the case of the Landers rupture, a mean value of 46±10% with a mean width of 154 m (Milliner et al., 2015). Off-fault deformation for Camp Rock is not considered very high, assumed to be ≤20% (Milliner et al., 2015).Our study area combines several characteristics that are favorable to obtain a geological long term slip-rate: 1) is a preserved valley, where little deposition or erosion has occurred since a given time; OFD is assumed to be ≤20%; 3) surface expression of the fault is clear and simple; 4) the fault displaces geology/ morphology easily recognized.

We estimate a slip-rate of $0.6^{+3}/_{-0.3}$ mm/a for the Graben section, and we show that despite this section did not completely ruptured during the Landers earthquake, the fault has likely experience movement since the latest Pleistocene. Several right deflected and deeply incised creek channels provide evidence of recent tectonic activity and uplift, which is higher than at Camp Mine study area. A patch of CR2 is present along part of the Camp Rock fault that ruptured during the Landers earthquake, near the termination of the fault. However, it was not possible to recognize a correlative CR2 surface cross the fault trace in remote sensing or field survey to infer associated displacement.

Estimated displacements for the CR2 surface along the Camp Mine study area vary widely. The smallest displacement, 299±35 m, provides a slip rate of $1.1^{+0.3}/_{-0.2}$ mm/a, which is consistent with the slip-rate of ≤1.4±0.6 mm/a of Oskin et al. (2008) estimated for the last ~50 ka. This reconstruction is based in the alignment of a group of CR2, some drainages and the alignment of an alluvial fan lobe with a canyon source. However, we note that not all the surfaces CR2 were reconstructed and the alluvial fan probably has an age younger than CR2 and possibly within the same age range as the geomorphic elements studied by Oskin et al. (2008).

The largest estimated displacement of 1384±48 m provides a slip-rate of $4.9^{+1.9}/_{-1.1}$ mm/a, which is in the range of ≤3.2±0.4 mm/a, the slip-rate inferred for the Calico fault by Xie et al. (2018). This second reconstruction is based on the alignment of the majority of the CR2 surfaces and topographic alignment of the larger alluvial fan apex with the windgaps. We hypothesize that this larger size geomorphic feature is related with larger size sediment sources that can provide the focused volume of sediment. This reconstruction also aligns a topographical high that was interpreted to be an anomalous higher uplift point in the proximity of the fault (Kaneda and Rockwell, 2009). Kaneda and Rockwell propose a kinematic model where the uplift is associated with a right stepping double bend. According to their Coulomb stress modeling, the deformation in the topography will only generate under specific fault geometry and kinematics; the fault planes distanced 50 m in the surface and merging at a depth of 140m, a fault having a minor reverse component, in particular with a 20° rake. We suggest that although some localized vertical deformation might be present, it might have built upon pre-existent higher alluvial fan morphology where drainage had inset earlier, associated with a CR2 patch. Because this largest displacement realigns most of the CR2 patches and the paleo drainage pattern, it is the preferred option for a CR2 reconstruction. However, together with the surface age estimated it provides a very high slip rate that seems unrealistic for our geomorphologic observations. The fault expression is straight, with several geomorphic indicators of continuous activity, however, presents a smoothened morphology and degraded scarps which are not supportive of such a high latest Pleistocene-Holocene slip-rate. In addition, Holocene earthquakes are more indicative of a slip-rate in the range of 1–2 mm/a rather than a slip rate in the range of 5 mm/a.

Both slip-rates estimates are within the geodetic rate of 0.5–4.7 mm/a proposed by Evans et al. (2016) for the Camp Rock, although we note that our higher slip rate estimate of$4.9^{+1.9}/_{-1.1}$ mm/a falls into the higher end. The lower estimate is similar with the one from Oskin et al. (2008) and suggests a much lower geological rate than the geodetic. We will briefly discuss the likelihood of a higher or lower geological slip rate in our study area.

The OFD conditions strain accommodation at the main fault zone and influence geological slip rates. The magnitude and widths of OFD are recognized to be controlled by several factors, the structural complexity of the fault system being the primary one, the existence of additional weakness structures, and finally the type of near-surface materials where a surface rupture occurs (Herbert et al., 2014b; Gold et al., 2015; Milliner et al., 2015).Consequently, OFD will be predominant and potentially larger along fault segments that present structural complexity and changes, such as stopovers, bends, and fault tips, while less complex segments with more defined and straight fault traces tend to have less OFD. The structural complexity in a fault system is assumed to be a decreasing function of the geological offset (Wesnousky, 1988, Stirling et al., 1996) and also relates with the degree of fault maturity; younger faults are characterized by discontinuous traces and increasing displacements tend to remove discontinuities.

The Camp Rock fault in the Camp Mine section is structurally less complex compared to the Graben section. Due to the fault structural simplicity and continuous straight fault trace (and relative maturity in comparison with other sections of the fault) we interpret that at the Camp Mine study area, the cumulative displacements may be more indicative of the strain accommodation and likely to present higher geological slip rates than other locations. Our estimate of a higher slip rate of $4.9^{+1.9}/_{-1.1}$ mm/a, although high falls it is within range of the geodetic rates determined by Evans et al. (2016) and may be indicative of a high kinematic efficiency.

An explanation for lower geologic slip rates than geodetic models refers to faults that may be exhibiting a "shallow slip deficit" (Fialko et al., 2005). The shallow slip deficit refers to a decrease of co-seismic displacement in the upper section of a fault (3–4 km)in comparison with the co-seismic displacement in depth estimated from the geodetic data such as slip inversions of near-field InSAR or a combination of InSAR and GPS data (e.g., Fialko et al., 2005; Kaneko and Fialko, 2011). Another parameter referring to slip deficit is the "surface slip ratio" (SSR) which is assumed to be a ratio between the average surface slip and the average slip at 3–6 km depth. Relationships between SSR and the geodetically inferred slip at depth were investigated for several continental strike-slip fault systems including the surface ruptures during the Landers and Hector Mine earthquakes (Dolan and Haravitch, 2014). A higher fault maturity correlates proportionally with both the coseismic and long-term cumulative displacement while a higher degree of complexity correlates inversely. SSR ratios are lower for the Landers and Hector Mine surface ruptures than the more mature faults (cumulative fault displacement ≥ 85 km). The SSR values for structural simple sections for Landers and Hector Mine surface ruptures range from 0.6–0.8 while for mature faults range from 0.7–0.9 (Fig.3 in Dolan and Haravitch, 2014). A value of SSR 0.6 is presented for our entire study area without differentiation between the structural simple Camp Mine and structural complex Graben section.

A consistent observed lack of coseismic slip for the upper part of a fault raises the question if this deficit can be compensated through time by interseismic creep and post-seismic after-slip, but this is still an open question. While Kaneko and Fialko (2011) argue that there is not enough data collected in surface ruptures to evaluate this hypothesis and model, Dolan and Haravitch (2014) suggest that most of the slip deficit is accommodated post-seismically, assuming an inelastic off-fault condition. The post-seismic adjustment in the upper may be compensated through the cycles of seismicity, suggesting that long term slip rates may include this adjustment. As such, long term geological slip rates might be more representative of a fault system slip rate (Resor et al., 2018), as is the case of Camp Mine study area.

The differences in our results from Camp Mine section suggest: a higher displacement associated with a $279^{+80}/_{-78}$ ka period with a of slip rate $4.9^{+1.9}/_{-1.1}$ mm/a and a lower displacement, that may have occurred since $279^{+80}/_{-78}$ ka period or much later (likely to be MIS 6 or younger). In the case, that the smaller displacement corresponds to a period of time lesser than ~180 ka, then the slip rate could be in the range of 1.5–2 mm/a. Holocene and late Pleistocene geomorphic and geological data suggest a slip rate of ~1 mm/a. These results suggest a decrease in the slip rate through time, however needs corroboration from additional data.

We proposed that the slip-rates for the Camp Rock fault, namely in the Camp Mine section might have some slip-rate variability through time similarly to other tectonic settings(i.e., Cowie et al., 2012; Elliot et al., 2018; Khajavi et al., 2018; Zinke et al., 2018). Those can be related with several mechanisms such as fault or segment interactions, non-constant kinematic efficiency, fault re-organization, among others.

Assuming a geodetic steady state condition with accommodation of 10–12 mm/a for the entire ECSZ, the discrepancy between the geologic and geodetic rates may be related with fault reorganization through time. Evidence of changes of slip-rate during late Quaternary may suggest a transfer of accommodation where additional structures besides the main Camp Rock fault are presently accommodating strain.

The slip-rate decrease from the Camp Mine to the Emerson section is mostly due to strain accommodation within the graben by the Camp Rock and Emerson faults as well as to the termination of the Camp Rock fault.

6. Conclusions

The Camp Rock fault is a straight right-lateral strike-slip fault zone, with two discontinuous sub-parallel branches. There is evidence of right lateral and subtle of reverse faulting, which includes linear valleys, scarps, and right deflected channels. We obtained numerical ages for two surfaces, CR2 with an age of $278^{+80}/_{-78}$ka and CR3 with an age of $351^{+157}/_{-123}$ ka and evidence for another minor depositional period at ~155–165 ka. We calculate a slip rate of $0.6^{+3}/_{-0.3}$ mm/a for the termination of the Camp Rock fault along the graben with Emerson fault. For the Camp Mine study area we calculate two possible slip rates of $1.1^{+0.3}/_{-0.2}$ mm/a and another one of $4.9^{+1.9}/_{-1.1}$,based on the same surface displacement and two different scenarios that have displacements of 299±35 and 1384±48 m, respectively. However, we consider that the two displacements at Camp Mine can be representative of displacement for different time ranges, based on geomorphology interpretation, meaning that we calculate a slip rate of $4.9^{+1.9}/_{-1.1}$ for $278^{+80}/_{-78}$ ka, and likely slip rate in the range of 1.5–2 mm/a for a probable period < ~180 ka.

These results contribute for the recognition of slip-rate variability through time and space for one of the major active structures in the MECSZ which can be indicative of active faulting reorganization since late Pleistocene, with implications regarding the regional strain accommodation knowledge. The geological slip rate variability since late Pleistocene and the assumption of a geodetic steady rate slip rate suggests that new active structures are forming or that older ones are being reactivated. Surface ruptures occurring in multiple structures as during the Landers and Hector Mine earthquakes, which in the MECSZ occurred in clusters through time may be indicative of fault reorganization. Characterizing the seismic hazard in MECSZ based on one timeframe may be problematic and underestimate seismic potential in additional structures.

Acknowledgments This work was funded under USGS NEHRP Cooperative Agreement G18AP00065 & G18AP00066.

Data: The data produced will be available upon request to the PI's and through peer-review publication (a manuscript is being prepared).

Publications: An early version of this research was presented in AGU 2019 Fall Meeting (Figueiredo et al. 2019).

Figueiredo, P.M., Wetmore, P., Rasmussen, C., Owen, L.A., Votor, A., Dixon, T., 2019 Long term slip rate of Camp Rock Fault (Eastern California Shear Zone) and implications for the regional understanding of geological rates. AGUFM 2019, T51B-04, Oral presentation at 2019 AGU Fall Meeting.

A manuscript for publication is being prepared and will be submitted soon.

7. References

Andrew, J.A. and Walker, J.D., 2017. Path and amount of dextral fault slip in the Eastern California shear zone across the central Mojave Desert, GSA Bulletin, 7/8; p. 855–868; doi: 10.1130/B31527.1

Balco, G., Stone, J.O., Lifton, N., and Dunai, T.J., 2008. A complete and easily accessible means of calculating surface exposure ages or erosion rates from 10Be and 26Al measurements. Quat. Geochron. 3, 174-195.

Balco, G., 2017. Production rate calculations for cosmic-ray-muon-produced ^{10}Be and ^{26}Al benchmarked against geological calibration data, Quaternary Geochronology, V., 150-173.

Barbot, S., Fialko,Y., Sandwell,D., 2008. Effect of a compliant fault zone on the inferred earthquake slip distribution. J.Geophys.Res.113,B06404.

Bird, P., 2007, Uncertainties in long-term geologic offset rates of faults: General principles illustrated with data from California and other western states: Geosphere, v. 3, p. 577–595, doi: 10 .1130 /GES00127 .1.

Bryant, W.A., compiler, 2000. Fault number 114a, Camp Rock-Emerson-Copper Mountain fault zone, Camp Rock section, in Quaternary fault and fold database of the United States: U.S. Geological Survey website, http://earthquakes.usgs.gov/hazards/qfaults, accessed 04/19/2016.

Bull, W.B., 1977. The alluvial-fan environment. Prog. Phys. Geogr. 1, 222-270.

Bull, W., 1979. Tectonic geomorphology of the Mojave Desert, California: U.S. Geol. Survey Preliminary Rept. (manuscript), Contract No. 14-08-00001-G-394, 188 p.

Bull, W.B., 1991. Geomorphic Responses to Climate Change. Oxford University Press, New York.

Bull, W.B., 1996. Global climate change and active tectonics: effective tools for teaching and research, Geomorphology, 16, 217-232.

Cowie, P.A., Roberts, G.P., Bull, J.M., Visini, F., 2012. Relationships between fault geometry, slip rate variability and earthquake recurrence in extensional settings, Geophys. J. Int. 189, 143–160, doi: 10.1111/j.1365-246X.2012.05378.x.

Dibble, T.W. Jr., 1964. Geologic map of the Rodman Mountains quadrangle, San Bernardino County, California: U. S. Geol. Survey Misc. Geol. Investigations Map 1-430.

Dixon, T.H., Robaudo, S., Lee, J., and Reheis, M.C., 1995, Constraints on present-day Basin and Range deformation from space geodesy: Tectonics, v. 14, p. 755-772, doi: 10.1029/95TC00931.

Dixon, T.H., and Xie, S., 2018, A kinematic model for the evolution of the Eastern California Shear Zone and Garlock Fault, Mojave Desert, California: Earth and Planetary Science Letters, v. 494, p. 60–68. doi:10.1016/j. epsl.2018.04.050.

Dokka, R.K., 1983. Displacements on late Cenozoic strike-slip faults of the central Mojave Desert, California, Geology 11, 305-308.

Dokka, R.K., and Travis, C.J., 1990, Late-Cenozoic strike-slip faulting in the Mojave, Desert, California: Tectonics, v. 9, p. 311-340.

Dolan, J.F., Bowman, D.D., and Sammis, C.G., 2007, Long-range and long-term fault interactions in southern California: Geology, v. 35, p. 855-858, doi: 10.1130/G23789A.1.

Dolan, J.F., and Haravitch, B.D., 2014, How well do surface slip measurements track slip at depth in large strike-slip earthquakes? The importance of fault structural maturity in controlling on-fault slip versus off-fault surface deformation, Earth and Planetary Science Letters, v. 388, p. 38–47. doi:10.1016/j.epsl.2013.11.043.

Elliott, A.J., Oskin, M.E., Liu-zeng, J., Shao Y.-X., 2018. Persistent rupture terminations at a restraining bend from slip rates on the eastern Altyn Tagh Fault, Tectonophysics, 733, 57-72, doi.org/10.1016/j.tecto.2018.01.004.

Eppes, M.C., McDonald, E.V., and McFadden, L.C., 2003. Soil geomorphology studies in the Mojave Desert: Impacts of Quaternary tectonics, climate, and rock type on soils, landscapes, and plant community ecology: in Easterbrook, D. J., ed., Quaternary Geology of the United States [INQUA 2003 Field Guide Volume], 1-18.

Evans, E. L.,Thatcher, W. R., Pollitz, F. F., Murray, J. R., 2016. Persistent slip rate discrepancies in the eastern California (USA) shear zone. Geology, 44; no. 9; p. 691–694.

Frankel, K.L., Glazner, A.F., Kirby, E., Monastero, F.C., Strane, M.D., Oskin, M.E., Unruh, J.R., Walker, J.D., Anandakrishnan, S., Bartley, J.M., Coleman, D.S., Dolan, J.F., Finkel, R.C., Greene, D., Kylander-Clark, A., Marrero, S., Owen, L.A., and Phillips, F., 2008. Active tectonics of the eastern California shear zone, *in* Duebendorfer, E.M., and Smith, E.I., eds., Field Guide to Plutons, Volcanoes, Faults, Reefs, Dinosaurs, and Possible Glaciation in Selected Areas of Arizona, California, and Nevada: Geological Society of America Field Guide 11, p. 43–81, doi: 10.1130/2008.fl d011(03).

Fialko, Y., Sandwell, D., Simons, M., Rosen, P., 2005.Three-dimensional deformation caused by the Bam, Iran, earthquake and the origin of shallow slip deficit. Nature 435, 295–299. http://dx.doi.org/10.1038/nature03425.

Gan, W., Svarc, J.L., Savage, J.C., Prescott, W.H., 2000. Strain accumulation across the Eastern California shear zone at latitude 36◦30N, J.Geophys.Res.105,16229–16236.

Gan, W. J., P. Zhang, and Z. K. Shen, 2003. Initiation of deformation of the eastern California shear zone: Constraints from Garlock fault geometry and GPS observations, Geophys. Res. Lett., 30(10), 1496, doi:10.1029/2003GL017090.

Ganev, P.N., Dolan, J.F., Blisniuk, K., Oskin, M., and Owen, L.A., 2010.Paleoseismologic evidence for multiple Holocene earthquakes on the Calico Fault: Implications for earthquake clustering in the Eastern California shear zone: Lithosphere, v. 2, no. 4, p. 287–298. doi:10.1130/L82.1.

Gile, L.H., 1961. A classification of Ca horizons in soils of a desert region, Dona Ana County, New Mexico 1. Soil Sci. Soc. Am. J. 25, 52. http://dx.doi.org/10.2136/sssaj1961. 03615995002500010024x.

Gile, L.H., Hawley, J.W. & Grossman, R.B. 1981. Soils and geomorphology in the Basin and Range area of southern New Mexico; guidebook to the Desert Project. New Mexico Bureau of Mines and Mineral Resources, Memoir 39.

Gold, R.D., Reitman, N.G., Briggs, R.W., Barnhart, W.D., Hayes, G.P., and Wilson, E., 2015, On-and off-fault deformation associated with the September 2013 Mw 7.7 Balochistan earthquake: Implications for geologic slip rate measurements: Tectonophysics, v. 660, p. 65–78, https:// doi .org /10 .1016 /j .tecto .2015 .08 .019.

Haddon, E.K., Miller, D.M., Langenheim, V., Mahan, S.A., 2019. Distributed fault slip in the eastern Californiashear zone: adding pieces to the puzzle nearBarstow, California, 2019 Desert Symposium ProceedingsVolume134-139.

Harden, J.W., 1982. A quantitative index of soil development from field descriptions: Examples from a chronosequence in central California: Geoderma, v. 28, no. 1, p. 1–28. doi:10.1016/0016-7061(82)90037-4.

Harden, J.W., Taylor, E.M., Hill, C., Mark, R.K., McFadden, L.D., Reheis, M.C., Sowers, J.M., and Wells, S.G., 1991. Rates of soil development from four soil chronosequences in the southern Great Basin: Quaternary Research, v. 35, no. 3–Part1, p. 383–399. doi:10.1016/0033-5894(91)90052-7

Hawkins, H.G., 1976. Strike-slip displacement along the Camp Rock Fault, Central Mojave Desert, San Bernardino, California, MSc. Thesis, University of Southern California, 63 p. and 3 plates.

Herbert, J.W., Cooke, M.L., and Marshall, S.T., 2014a. Influence of fault connectivity on slip rates in southern California: Potential impact on discrepancies between geodetic derived and geologic slip rates, Journal of Geophysical Research, p. 2342-2361, doi: 10.1002/2013JB10472.

Herbert, J.W., Cooke, M.L., Oskin, M., and Difo, O., 2014b. How much can off-fault deformation contribute to the slip rate discrepancy within the eastern California shear zone, Geology, v, 42, p. 71-74, doi: 10.1130/G34738.1

Hidy, A.J., Gosse, J.C., Pederson, J.L., Mattern, J.P., and Finkel, R. C., 2010. A geologically constrained Monte Carlo approach to modeling exposure ages from profiles of cosmogenic nuclides: An example from Lees Ferry, Arizona: Geochemistry, Geophysics, Geosystems, 1. 9 (code v1.2). doi:10.1029/2010GC003084.

Jachens, R.C., Langenheim, V.E., Matti,J.C., 2002. Relationship of the 1999 Hector Mine and 1992 Landers Fault Ruptures to Offsets on Neogene Faults and Distribution of Late Cenozoic Basins in the Eastern California Shear Zone, Bulletin of the Seismological Society of America, 92, 4, pp. 1592–1605.

Jennings, C.W. and Bryant, W.A., 2010. Fault Activity Map of California, California Geological Survey, 1/750 000.

Kaneda, H. and Rockwell, T.K., 2009. Triggered and Primary Surface Ruptures along the Camp Rock Fault, Eastern California Shear Zone, Bulletin of the Seismological Society of America, Vol. 99, No. 5, pp. 2704–2720, October 2009, doi: 10.1785/0120080310.

Kaneko, Y and Fialko, Y., 2011. Shallow slip deficit due to large strike-slip earthquakes in dynamic rupture simulations with elasto-plastic off-fault response, Geophys. J. Int. 186, 1389–1403, doi: 10.1111/j.1365-246X.2011.05117.x

Klinger, Y., Etchebes, M., Tapponnier, P., Narteau, C., 2011. Characteristic slip for five great earthquakes along the Fuyun fault in China, Nature Geoscience, 4, 389-392, DOI: 10.1038/NGEO1158.

Khajavia, N., Nicola, A., Quigleyb, M.C., Langridge, R.M., 2018. Temporal slip-rate stability and variations on the Hope Fault, New Zealand, during the late Quaternary, Tectonophysics 738–739, 112-123, doi.org/10.1016/j.tecto.2018.05.001.

Lal, D., 1991. Cosmic ray labeling of erosion surfaces: in situ nuclide production rates and erosion models. Earth and Planetary, Science Letters 104, 424–439.

Lifton, N., Sato, T., Dunai, T.J., 2014. Scaling in situ cosmogenic nuclide production rates using analytical approximations to atmospheric cosmic-ray fluxes. Earth and Planetary Science Letters 386, 149–160.

Lifton, 2016. Implications of two Holocene time-dependent geomagnetic models for cosmogenic nuclide production rate scaling, Earth and Planetary Science Letters, V. 433, 257-268.

Lowenstein, T. K., J. Li, C. B. Brown, S. M. Roberts, T. L. Ku, S. Luo, and W. Yang, 1999. 200 k.y. paleoclimate record from Death Valley salt core, Geology, 27, 3–6, doi.org/10.1130/0091-7613(1999)027<0003:KYPRFD>2.3.CO;2.

Manson, M., W., 1988. Camp Rock, Emerson, Galway Lake, Homestead Valley (north end) and associated faults, San Bernardino, California Division of Mines and Geology Fault Evaluation Report, FER-183.

Marrero, S.M., Phillips, F.M., Borchers, B., Lifton, N., Aumer, R., Balco, G., 2016. Cosmogenic nuclide systematics and the CRONUScalc program. Quaternary Geochronology 31, 160-187.

Martin, L.C.P., Blard, P-H., Balco, G., Lavé, J., Delunel, R., Lifton, N., Laurent, V., 2017. The CREp program and the ICE-D production rate calibration database: A fully parameterizable and updated online tool to compute cosmic-ray exposure ages. Quaternary Geochronology 38, 25–49.

McFadden, L.W., 1982. The impacts of temporal and spatial climatic changes on alluvial soils genesis in southern California [Ph.D. dissert.]: Tucson, Arizona, University of Arizona, 430 p..

McGill, S., Spinler, J., McGill, J., Bennet, R., Floyd, M., Fryxell, J. and Funning, G., 2015, Kinematics modeling of fault slip rates across the Pacific-North America plate boundary through the San Bernardino Mountains, California, Journal of Geophysical Research, , v.120, p. 2772-2793, doi:10.1002/2014JB011459.

Miller, F. K., and D. M. Morton, 1980. Potassium–argon geochronology of the eastern Transverse Ranges and southern Mojave Desert, southern California, U.S. Geol. Surv. Profess. Pap. 1152.

Miller, D.M., 2017. The late Cenozoic Eastern California Shear Zone after 25 years of study, 2017 Desert Symposium Proceedings Volume, 45-54.

Miller, M.M., Johnson, D.J., Dixon, T.H., and Dokka, R.K., 2001, Refined kinematics of the eastern California shear zone from GPS observations, 1993-1994: Journal of Geophysical Research, v. 106, p.2245-2263, doi:10.1029/2000JB900328.

Miller, D.M., Cyr, A., Menges, C., Schmidt, K.M., Mahan, S.A., Maher, K., Liu, T., 2015. The Pleistocene climate record in alluvial fans of the Mojave desert, Quaternary International 387, 139-140.

Milliner, C.W., Dolan, J.F., Hollingsworth, J., Leprince, S., Ayoub, F., and Sammis, C.G., 2015, Quantifying near-field and off-fault deformation patterns of the 1992 Mw 7.3 Landers earthquake: Geochemistry, Geophysics, Geosystems, v. 16, p. 1577–1598, https:// doi .org /10 .1002 /2014GC005693.

NASA/METI/AIST/Japan Spacesystems, and U.S./Japan ASTER Science Team. ASTER Global Digital Elevation Model V003. 2019, distributed by NASA EOSDIS Land Processes DAAC, https://doi.org/10.5067/ASTER/ASTGTM.003. Accessed 2019-10-01.

Nishiizumi, K., Imamura, M., Caffee, M.W., Southon, J.R., Finkel, R.C., Mcaninch, J., 2007. Absolute calibration of 10Be AMS standards. Nuclear Instruments and Methods in Physics Research Section B: Beam Interactions with Materials and Atoms 258, 403–413.

Nur, A., Ron, H., Beroza, G., 1993. The nature of the Landers-Mojave earthquake line, Science, 261, 201-203.

Pérez-Peña, J.V., Alawabdeh, M.A., Azañón, J.M., Galve, J.P., Booth-Rea, G, Notti, D., 2016. SwathProfiler and NProfiler: Two new ArcGIS Add-ins for the automatic extraction of swath and normalized river profiles, Computers & Geosciences, V. 104, 135-150.

Oskin, M. and Perg, L, 2006. Fault systems in the California Shear Zone, CA, National Center for Airborne Laser Mapping (NCALM), distributed by OpenTopography, http://doi.org/10.5069/G93X84KG

Oskin, M., Perg, L., Blumentritt, D., Mukhopadhyay, S., and Iriondo, A., 2007, Slip rate of the Calico fault: implications of geologic versus geodetic rate discrepancy in the eastern California shear zone: Journal of Geophysical Research, v. 112, B03402, doi: 10.1029/2006JB004451.

Oskin, M., Perg, L., Shelef, E., Strane, M., Gurney, E., Singer, B., and Zhang, X., 2008, Elevated shear zone loading rate during an earthquake cluster in eastern California, Geology, v. 36, p. 507-510, doi: 10.1130/G24814A.1.

Perrin, C., I. Manighetti, J.-P. Ampuero, F.Cappa, and Y. Gaudemer, 2016. Location of largest earthquake slip and fast rupture controlled by along-strike change in fault structural maturity due to fault growth, J. Geophys. Res. Solid Earth, 121, 3666–3685, doi: 10.1002/2015JB012671.

Phelps, G.A., Bedford, D.R., Lidke, D.J., Miller, D.M., and Schmidt, K.M., 2012, Preliminary surficial geologic map of the Newberry Springs 30’ x 60’ quadrangle, California: U.S. Geological Survey Open-File Report 2011–1044, pamphlet 68 p., 1 sheet, scale 1:100,000. (Available at https://pubs.usgs.gov/of/2011/1044/.)

Ponti, D., and others (2020, in review). Documentation of surface fault rupture and ground deformation features produced by the Ridgecrest M6.4 and M7.1 earthquake sequence of July 4 and 5, 2019, Seismol. Res. Letters.

Reheis, M.C., Bright, J., Lund, S.P, Miller, D.M., Skipp, G., Fleck, R.J., 2012. A half-million-year record of paleoclimate from the Lake Manix Core, Mojave Desert, California, Palaeogeography, Palaeoclimatology, Palaeoecology 365–366, 11–37. doi.org/10.1016/j.palaeo.2012.09.002.

Resor, P. G., Cooke, M.L., Marshall, S.T., Madden, E.H., 2018. Influence of Fault Geometry on the Spatial Distribution of Long-Term Slip with Implications for Determining Representative Fault-Slip Rates, Bull. Seism. Soc. Am, 108 (4), 1837–1852, doi: 10.1785/0120170332

Rockwell, T.K., Lindvall, S., Herzberg, M., Murbach, D., Dawson, T. and Berger, G., 2000. Paleoseismology of the Johnson Valley, Kickapoo, and Homestead Valley Faults: Clustering of Earthquakes in the Eastern California Shear Zone, Bull. Seism. Soc. Am., 90, 5, 1200-1236.

Sauber, J., Thatcher, W., Solomon, S.C., and Lisowski, M., 1994, Geodetic slip rate for the eastern California shear zone and the recurrence time of Mojave desert earthquakes: Nature, v. 367, p. 264-266, doi: 10.1038/367264a0.

Savage, J.C., Lisowski, M., and Prescott, 1990, An apparent shear zone trending north-northwest across the Mojave Desert into Owens Valley, California, Geophysical Research Letters, v. 17, p. 2113-2116.

SCAMP,Southern California Areal Mapping Project, 2000, A proposed classification for surficial geologic materials in southern California, version 1.0.: U.S. Geological Survey, Open-File Report.

Selander, J.A., 2015. Mechanisms of Strain Transfer Along Strike---Slip Faults: Examples from the Mojave Desert, California, Doctoral Dissertation, University of California, Davis, 166 p.

Shelef, E., and Oskin, M., 2010, Deformation processes adjacent to active faults: Examples from eastern California: Journal of Geophysical Research: Solid Earth, v. 115, no. B5. doi:10.1029/2009JB006289.

Shepard, C., Pelletier, J. D., Schaap, M. G., & Rasmussen, C. (2018). Signatures of obliquity and eccentricity in soil chronosequences. Geophysical Research Letters, 45, 11,147–11,153. doi. org/10.1029/2018GL078583.

Shlemon, R.J., 1980, Age of faulting, Lucerne Valley Generating Station (Upper Johnson Valley), San Bernardino county, California: Newport Beach, R,J, Shlemon and Associates, Inc., unpublished consulting report prepared for southern California Edison Company, 64p. (A-P file iC-626).

Sieh, K., Jones, L., Hauksson, E., Hudnut, K., Éberhart-Philips, D., Heaton, T., Hough, S., Hutton, K., Kanamori, A., Lilje, A., Lindrall, S., McGill, S., Mori, J., Rubin, C., Spotila, J., Stock, J., Thio, H.K., Treiman, J., Wernicke, B., Zachariasen, J., 1993. Near-field investigations of the Landers earthquake sequence, April to July, 1992, Science, 260, 171-176.

Spinler, J.C., Bennett, R.A., Anderson, M.L., McGill, S.F., Hreinsdóttir, S., and McCallister, A., 2010, Present-day strain accumulation and slip rates associated with southern San Andreas and eastern California shear zone faults: Journal of Geophysical Research: Solid Earth, v. 115, no. B11. doi:10.1029/2010JB007424.

Southern California Areal Mapping Project (SCAMP), 2000. A proposed classification for surficial geologic materials in southern California, version 1.0.

Stirling, M. W., S. G. Wesnousky, and K. Shimazaki (1996), Fault trace complexity, cumulative slip, and the shape of the magnitude-frequency distribution for strike-slip faults: A global survey, Geophys. J. Int., 124, 833 – 868.

Stone, J.O., 2000. Air pressure and cosmogenic isotope production. Journal of Geophysical Research: Solid Earth 105, 23, 753– 23,759.

Takaku, J., Tadono, T., Tsutsui, K., 2014. Generation of High Resolution Global DSM from ALOS PRISM. The International Archives of the Photogrammetry, Remote Sensing and Spatial Information Sciences, pp.243-248, Vol. XL-4, ISPRS TC IV Symposium, Suzhou, China, 2014.

Treiman, J., Kendrick, K.J., Bryant, W.A., Rockwell, T.K., McGill, S.F., 2002. Primary surface rupture associated with the M7.116 October 1999 Hector Mine earthquake, San Bernardino County, California. Bull. Seismol. Soc. Am. 92(4), 1171–1191.

Wesnousky, S.G.,1988.Seismological and structural evolution of strike-slip faults. Nature, 335,340–343.

Western Region Climate Center, http://www.wrcc.dri.edu

Woodburne, M.O., 2015, Mojave Desert Neogene tectonics and the onset of the Eastern California Shear Zone, in Reynolds, R.E., ed., Mojave Miocene: The 2015 Desert Symposium Field Guide and Proceedings, California State University Desert Studies Consortium, p. 153-199.

Xie, S., Gallanta, E., Wetmore, P., Figueiredo, P.M., Owen, L.A., Rasmussen, C., Malservisia, R. and Dixon T.H. 2018. A new geological slip rate estimate for the Calico Fault, eastern California: implications for geodetic versus geologic rate estimates in the Eastern California Shear Zone, International Geology Review, doi.org/10.1080/00206814.2018.1531272.

Zechar, J.D., and Frankel, K.L., 2009, Incorporating and reporting uncertainties in fault slip rates: Journal of Geophysical Research, v. 114, B12407, doi: 10 .1029 /2009JB006325.

Zielke, O., and J R. Arrowsmith, 2012. LaDiCaoz and LiDAR imager -MATLAB GUIs for LiDAR data handling and lateral displacement measurement*,* Geosphere 8, 206-221, doi:10.1130/GES00686.1.

Zielke, O., Klinger, Y., and Arrowsmith, J.R., 2015, Fault slip and earthquake recurrence along strike-slip faults—Contributions of high-resolution geomorphic data: Tectonophysics, v. 638, p. 43–62. doi:10.1016/j.tecto.2014.11.004.